Modelling of three-dimensional particle rebound from an anisotropic rough wall

Darko Radenkovic, Olivier Simonin

Modelling of three-dimensional particle rebound from an anisotropic rough wall

Darko Radenkovic [a,*], Olivier Simonin [b]

[a] University of Belgrade, Faculty of Mechanical Engineering, Belgrade, Serbia
[b] Institut de Mécanique des Fluides (IMFT), Université de Toulouse, CNRS, Toulouse, France

ARTICLE INFO

Article history:
Received 13 October 2020
Received in revised form 2 April 2021
Accepted 20 July 2021
Available online 27 July 2021

Keywords:
Anisotropic rough wall
Shadow effect
Virtual wall
Multiple particle-wall collisions
Three-dimensional particle rebound

ABSTRACT

In gas-solid confined flows, particle rebound on a rough wall may have a great influence on the macroscopic properties of both phases. Existing simulation methods use simplified approaches where surface roughness is modelled as two-dimensional or isotropic. To improve the accuracy of such simulations, an anisotropic virtual rough wall statistical approach and the corresponding Lagrangian stochastic particle-wall collision model are proposed. From deterministic simulations of the impact of particles on the anisotropic virtual wall given as correlated bi-Gaussian surface, wall-normal vector angle statistics are used for model development. Rebound angle statistics computed from deterministic simulations and using the proposed stochastic model are in very good agreement. Incident particles in vertical planes not collinear with one of the principal directions of the anisotropic rough surface are bouncing with a mean transverse angle towards the principal direction of lower roughness.

1. Introduction

Wall-confined particle-laden turbulent flows are frequently encountered in various fields of industry, such as in the pneumatic conveying of powders, in fluidized beds and in pollution control devices. In these flows, confinement with rough boundaries can significantly influence the properties of both phases [1,2]. The main effect of rough walls in particle-laden flows is redispersion of the particles. This effect depends on mechanisms that control particle motion, such as particle inertia, gravitational settling and inter-particle collisions [3,4].

Machined surfaces are usually rough owing to the manufacturing process. Depending on the directional properties, surfaces can have an isotropic roughness distribution (with the same roughness patterns in different directions) or, more often in engineering, an anisotropic roughness distribution (with different roughness patterns in different directions). For example, surfaces with isotropic roughness are manufactured using electro-chemical machining, abrasive jet machining and multi-directional surface milling, whereas anisotropic surfaces are created using turning, shaping and drilling processes [5]. Further, during exploitation, surfaces can become roughened owing to erosion or corrosion due to ageing.

In pure fluid turbulent flow, it has been found that surface anisotropy is an important parameter that influences skin friction and anisotropy of Reynolds stresses [6].

Owing to the particle incident angles and rough wall geometry, particle-rough wall interactions are usually three-dimensional (3D). However, in previous studies, a significant number of simplified models for particle-wall interactions in a Lagrangian frame have been proposed as two-dimensional (2D) [7,8,9,10,11,12,11] and 3D simplified models [13,14,15]. Improving the models for particle-rough wall interactions with respect to surface anisotropy can lead to more accurate numerical predictions of these flows.

Also, more detailed models for particle-rough wall interactions can support more accurate CFD-based erosion studies used to optimize the design of piping equipment with respect to erosion or to estimate locations in pipelines that are most prone to erosion [16,17,18,19,20,21].

In early studies of mechanisms to suspend particles in pneumatic conveying, Matsumoto and Saito [22] proposed a 2D model for the rebound of ellipsoidal particles from a smooth surface and then in a subsequent study [23] a 2D model for the rebound of spherical particles from rough wall was developed, in which the wall was modelled with a sine function. It was found that non-sphericity of the particles and wall roughness lead to an increase in the particle wall-normal rebound velocity.

In order to account for the irregular particle rebound from a rough wall, a stochastic 2D virtual wall concept was proposed for the first time by Tsuji et al. [7]. When the particle centre reaches a distance half of the particle diameter from the smooth wall boundary, if the particle incident angle is smaller than a certain value, the actual wall is replaced with a smooth "virtual" inclined wall. Further, the impact of a particle with this virtual wall is calculated according to a hard-sphere model for particle-wall collisions. Also in that study, parameters that

* Corresponding author.
E-mail address: dradenkovic@mas.bg.ac.rs (D. Radenkovic).

https://doi.org/10.1016/j.powtec.2021.07.055
0032-5910/

determine the virtual wall inclination were empirical and valid only for pipe flows with the examined experimental configuration. The model was later modified in [24] for the case of particle-laden channel flows.

To include the influence of particle collision with the three-dimensional wall roughness in numerical Euler-Lagrangian simulation of particle-laden flow in a horizontal pipe, in a study of Sommerfeld and Zivkovic [25] when particle collided with a wall, a virtual wall was generated with an inclination that obeyed Gaussian distribution. This virtual wall was then rotated around the vertical axis by an angle that obeyed continuous uniform distribution, assuming no preferential direction of roughness. If particle after collision with the virtual wall did not return into the flow, a virtual wall was generated again and the particle-wall collision process was repeated.

The results of experimental investigations of the rebound of particles with different sizes/shapes from channel walls made of different materials were presented by Sommerfeld and Huber [8]. It was found that at large incident angles, the roughness inclinations seen by the particles obey a Gaussian distribution with zero mean and standard deviation that depends on the wall roughness structure and the particle diameter. At low incident angles, due to the incident perspective, the particles "see" positive roughness inclinations with a higher possibility than negative inclinations, which is called the shadow effect. To take this effect into account, a modified Normal distribution was proposed for the roughness angles seen by the particles. The application of this distribution gave simulated particle rebound angles that were in good agreement with those from experimental measurements, except that the predicted probability density function (PDF) of small rebound particle angles was significantly higher compared with the experimental results.

The reason for this discrepancy is that in the proposed model it is neglected that if a particle has a small positive rebound angle, it can collide again with some near-wall asperity and return to the flow with a higher rebound angle, as described by Konan et al. [26].

Application of the stochastic model of Sommerfeld and Huber [8] for the generation of rough wall inclinations seen by particles in the RANS-DPS of particle-laden flows through pipes [27] and channels [2] enabled reasonable agreement of the particle mean velocity and rms of particle velocity fluctuations with the results of experimental measurements.

Squires and Simonin [13] studied the influence of wall roughness on disperse phase properties in the LES-DPS of vertical particle-laden turbulent channel flow. The rebound of particles from smooth and 3D rough walls was treated as elastic and, to account for particle rebound from a rough wall, a stochastic procedure was used. In that procedure, virtual walls were determined with a normal vector $\mathbf{n} = [\sin(\phi)\cos(\theta), \cos(\phi), \sin(\phi)\sin(\theta)]$, where the angles ϕ and θ obey a Gaussian distribution with zero mean and standard deviations $\Delta\gamma$. If after rebounding from the wall the particle does not return to the flow, sampling of the virtual wall is repeated.

Using the property that the PDF of the rebound angles of particles that undergo only one collision with a wall is nearly the same as the PDF of the rebound angles of particles that experience multiple particle-wall collisions before their return to the flow, a stochastic procedure to model multiple particle-wall collisions was proposed by Konan et al. [9].

Konan et al. [28] examined the influence of wall roughness on the dispersed phase in particle-laden turbulent channel flow in a DPS-DES frame using both a shadow effect model and a multiple particle-rough wall collision model. Comparing the results of these simulations, it was shown that the shadow effect model alone makes the effects of wall roughness less pronounced since a large number of grazing particles is generated. To increase the dispersion induced by wall roughness and to obtain better agreement with experimental results, the statistical characteristic of roughness should be increased in the shadow effect model when neglecting the multiple collision effect.

A stochastic procedure in a Lagrangian framework to account for 3D particle rebound from an isotropic rough surface was proposed by Radenkovic and Simonin [29]. Using a deterministic simulation of the 3D particle impact on such a surface, it was found that the particle rebound angle in the bouncing plane and the probability that a particle makes only one rebound before returning to the flow are in agreement with the 2D stochastic approach of Konan et al. [9]. The transverse deviation angle obeys a zero mean Normal distribution with a standard deviation that increases with increase in the particle vertical incident angle.

In this paper, the interaction of particles with anisotropic walls is analysed and modelled as an extension of the 2D models of Sommerfeld and Huber [8] and Konan et al. [9] and the 3D model for the interaction of particles with isotropic walls of Radenkovic and Simonin [29]. The fluid influence on particle-wall collision processes is neglected in this study.

In order to support the derivation of a stochastic procedure for particle-rough wall interactions, deterministic simulations of the impact of particles on a rough wall are presented. These simulations enable us to isolate and study the effect of particle-wall interactions independently of other mechanisms that influence particle motion. These simulations are carried out from the perspective of the particle centre: wall inclination seen by the particle at the point of true particle-wall contact is assumed to be equivalent to the virtual wall inclination seen by the particle centre at the moment when the particle reaches the true wall [29].

The paper is organized as follows. In Section 2 the generation of a virtual anisotropic rough wall and the statistical characteristics of the corresponding virtual wall normal vector are described. The procedure for the deterministic simulation of particle impact on a rough wall is presented in Section 3. Also in that section a statistical analysis of particle rebound angles is carried out and virtual wall normal vector angles are modelled. As a result, a stochastic procedure for the calculation of 3D particle rebound from an anisotropic rough wall is obtained and the corresponding predictions of virtual wall normal vector angles viewed by incident particles are validated from the deterministic simulations results. The particle rebound angles obtained from available experimental results and deterministic and stochastic simulations are compared in Section 4.

2. Generation and properties of a virtual anisotropic rough wall surface

2.1. Description of Gaussian random rough surface generation

An anisotropic Gaussian rough surface, used here as a virtual rough wall, is generated according to Garcia and Stoll [30], implemented and freely available at [31].

To create this rough surface, random uncorrelated height values are generated at given Cartesian mesh nodes (x', z') in the x-z plane, obeying a Normal distribution with zero mean and standard deviation equal to the rms roughness height h. To achieve correlation length scales in the x and z principal directions, $c_{\mathrm{L},x}$ and $c_{\mathrm{L},z}$, respectively, a convolution of distribution $y_{\mathrm{u}}(x', z')$ is performed:

$$y(x,z) = \int_{-\infty}^{+\infty}\int_{-\infty}^{+\infty} f(x-x', z-z')\, y_{\mathrm{u}}(x', z')\, \mathrm{d}x'\mathrm{d}z' \tag{1}$$

where

$$f(x,z) = \frac{2}{\sqrt{\pi} c_{\mathrm{L},x} c_{\mathrm{L},z}} \exp\left(-\frac{2x^2}{c_{\mathrm{L},x}^2} - \frac{2z^2}{c_{\mathrm{L},z}^2}\right) \tag{2}$$

represents the anisotropic Gaussian filter.

Eq. (1) is calculated using a fast Fourier transform algorithm. An example of the anisotropic surface generated with this procedure is shown in Fig. 1. To achieve proper statistics, characteristic surface length scales

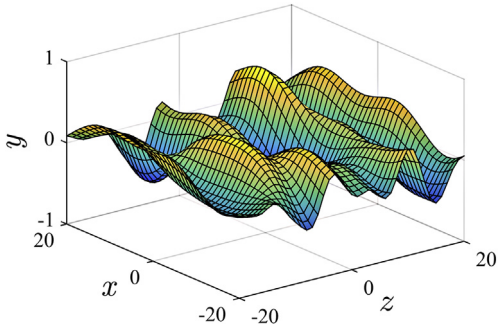

Fig. 1. Virtual anisotropic rough wall with rms roughness height $h = 0.37\mu$m and correlation length scales in the x and z principal directions of $c_{L,x} = 12\mu$m and $c_{L,z} = 4\mu$m, respectively. The mesh resolution is $\delta x = \delta z = 1\mu$m.

have to be sufficiently larger than the corresponding correlation length scales [31].

2.2. Characterization of the 3D virtual anisotropic rough wall normal vector

Let us introduce angles $(\xi,\eta,\zeta) \in [0,\pi]\ x[0,\pi/2]x[0,\pi]$, between the normal vector $\mathbf{n}$ of a virtual rough wall and direct basis vectors along the coordinate axes (Fig. 2).

The virtual normal vector $\mathbf{n}$ may be written as

$$\mathbf{n} = \cos(\xi)\mathbf{i} + \cos(\eta)\mathbf{j} + \cos(\zeta)\mathbf{k} \tag{3}$$

where $\mathbf{i}$, $\mathbf{j}$ and $\mathbf{k}$ are direct basis vectors in the direction of the x, y and z coordinate axes, respectively.

Let us assume that the angles ξ and ζ are random variables with mean values μ_ξ and μ_ζ and fluctuations ξ' and ζ', respectively:

$$\xi = \mu_\xi + \xi', \qquad \zeta = \mu_\zeta + \zeta' \tag{4}$$

and let us introduce standard deviations $\Delta\xi$ and $\Delta\zeta$ (or variances $\Delta\xi^2$ and $\Delta\zeta^2$), the covariance $\mathrm{Cov}(\xi,\zeta)$ and the correlation coefficient $\rho_{\xi\zeta}$:

$$\rho_{\xi\zeta} = \frac{\mathrm{Cov}(\xi,\zeta)}{\Delta\xi\Delta\zeta} \tag{5}$$

In the frame of low roughness approximation studied here we assume that the standard deviations of angles ξ and ζ (in radians) satisfy:

$$\Delta\xi \ll 1 \quad \text{and} \quad \Delta\zeta \ll 1 \tag{6}$$

Let us introduce angles ξ^*, η^* and ζ^* that the virtual normal vector $\mathbf{n}$ forms with the x^*, y^* and z^* axes, respectively, of the reference frame

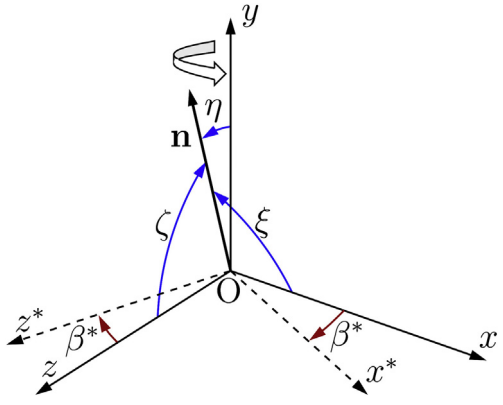

Fig. 2. Angles of the virtual wall normal vector $\mathbf{n}$ with direct basis vectors along the coordinate axes of reference frame $Oxyz$. Rotation of reference frame $Oxyz$ around the y-axis by an angle $\beta^* \in [-180°, 180°]$.

$Ox^*y^*z^*$ obtained by the rotation of reference frame $Oxyz$ around the y-axis by an angle $\beta^* \in [-180°, 180°]$ (Fig. 2). So, for $\beta^* = 0°$, it follows $\xi^* = \xi$, $\eta^* = \eta$ and $\zeta^* = \zeta$.

To examine the properties of these virtual wall normal vector angles along different x^* directions of numerically generated surface, scatter plots of angles (ξ^*, η^*), (ζ^*, ξ^*) and (ζ^*, η^*) are shown in Fig. 3 for $\beta^* \in [0°, 90°]$ and the corresponding correlation coefficients are given in Table 1.

The numerical surface examined has the equal length $L = 5$mm in the x and z direction, number of computational nods is 5001, rms roughness height is $h = 0.37\mu$m and correlation length scales in the x and z directions are $c_{L,x} = 12\mu$m and $c_{L,z} = 4\mu$m, respectively. Discretization points along direction defined with β^*, where the angles ξ^*, η^* and ζ^* are calculated, are distanced with step around 0.1μm. In these points, virtual wall normal vector is calculated as unit vector normal to triangular plane formed with surrounding heights in the computational nods and virtual normal vector angles are:

$$\xi^* = \arccos(n_{x^*}) \quad \eta^* = \arccos(n_{y^*}) \quad \zeta^* = \arccos(n_{z^*}) \tag{7}$$

The calculations of virtual wall normal vector angles ξ^* and ζ^* of numerically generated surface show that these two angles obey Normal distributions with mean values $\mu_{\xi^*} = \mu_{\zeta^*} = \pi/2$ along any direction determined with the angle β^*.

Table 1 shows that the correlation coefficients of the angles ξ^* and ζ^*,

$$\rho_{\xi^*\zeta^*} = \frac{\mathrm{Cov}(\xi^*,\zeta^*)}{\Delta\xi^*\Delta\zeta^*} \tag{8}$$

are nearly equal to zero when coordinate axes x^* and z^* (Fig. 2) are collinear with principal directions of roughness, i.e. the angle $\beta^* \in \{0°, 90°\}$ (or in opposite directions $\beta^* \in \{-90°, 180°\}$). In contrast, when coordinate axes x^* and z^* are non-collinear with principal directions of roughness, correlation coefficients of the angles ξ^* and ζ^* are different from zero.

In the frame of low roughness approximation given by Eq. (6), the variances and covariance of ξ^* and ζ^* for any β^* value may be computed directly in terms of the variances and covariance of ξ and ζ, corresponding to $\beta^* = 0°$, using the relations for the rotation of a frame $Oxyz$ by an angle β^* around the y-axis (Fig. 2),

$$\begin{aligned}
\Delta\xi^{*2} &= \cos^2(\beta^*)\Delta\xi^2 + \sin^2(\beta^*)\Delta\zeta^2 \\
\Delta\zeta^{*2} &= \sin^2(\beta^*)\Delta\xi^2 + \cos^2(\beta^*)\Delta\zeta^2 \\
\mathrm{Cov}(\xi^*,\zeta^*) &= \sin(\beta^*)\cos(\beta^*)\left[\Delta\xi^2 - \Delta\zeta^2\right]
\end{aligned} \tag{9}$$

Anisotropic roughness imposes the condition that variances of the angles ξ^* and ζ^* are different, $\Delta\xi^{*2} \neq \Delta\zeta^{*2}$.

Table 1 shows that the agreement of standard deviations $\Delta\xi^*$ and $\Delta\zeta^*$ and correlation coefficient $\rho_{\xi^*\zeta^*}$ given by Eq. (8) calculated with variances $\Delta\xi^{*2}$ and $\Delta\zeta^{*2}$ and covariance $\mathrm{Cov}(\xi^*,\zeta^*)$ from Eq. (9) and the corresponding values calculated from the numerically generated surface, is excellent, for different directions defined with the angle β^*.

Based on the values of the correlation coefficients $\rho_{\xi^*\zeta^*}$ and the shape of scatter plots, it can be concluded that the angles ξ^* and ζ^* are uncorrelated for principal directions of roughness whereas for directions non-collinear with principal directions of roughness, the angles ξ^* and ζ^* are correlated.

Fig. 3 shows that the angles η^* and ξ^* as well as the angles η^* and ζ^* are conditionally dependent variables although the corresponding correlation coefficients are nearly equal to zero. The statistical dependence measured between these random variables is due to the fact that they are linked analytically by the equation:

$$\cos^2(\xi^*) + \cos^2(\eta^*) + \cos^2(\zeta^*) = 1 \tag{10}$$

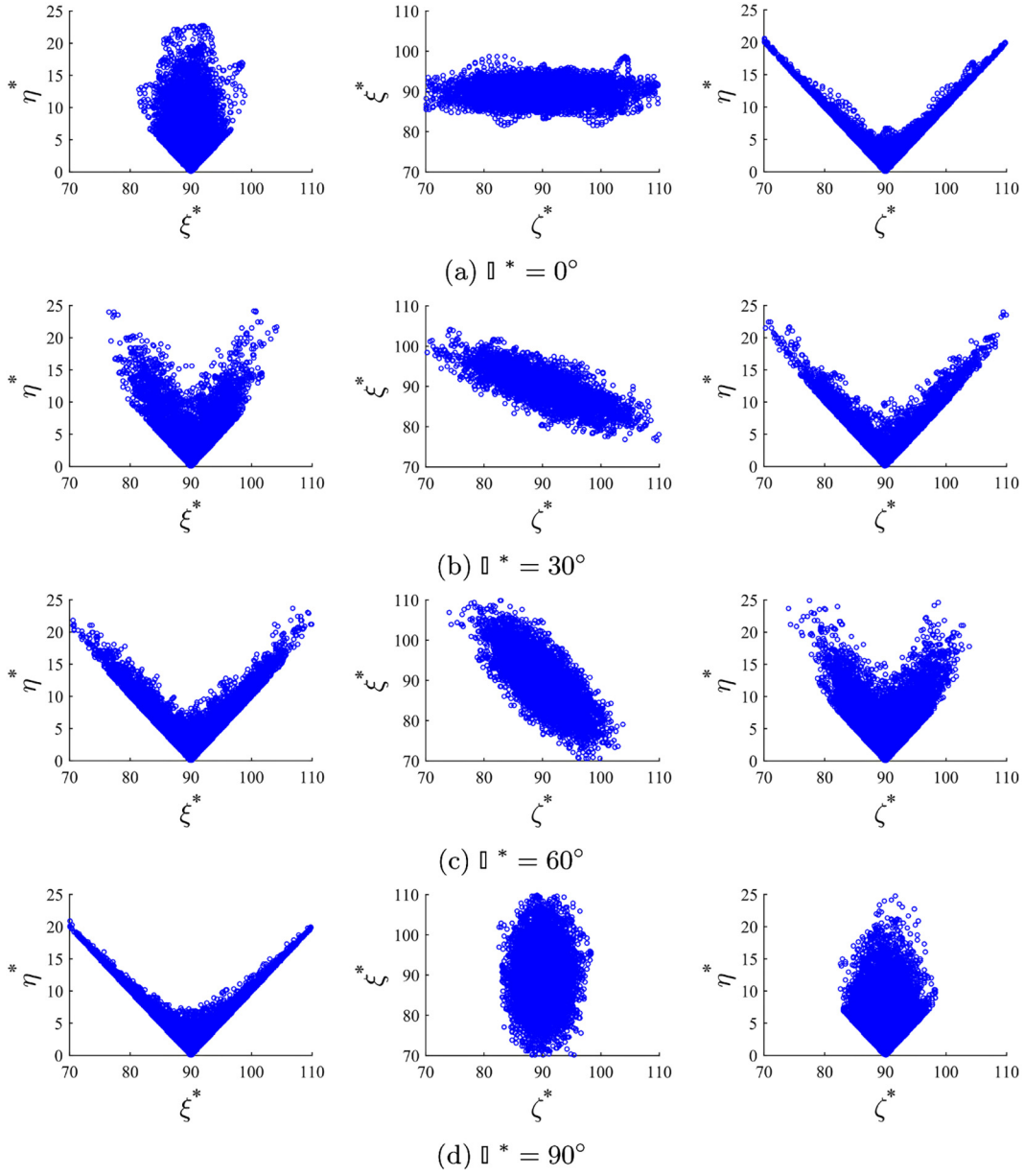

Fig. 3. Scatter plots of virtual wall normal vector angles ξ^*, η^* and ζ^* along the direction x^* defined with angle β^* for the numerically generated surface. Values on the axes are in degrees.

Table 1
Virtual wall normal vector angle characteristics calculated from a numerically generated virtual wall and statistical model Eq. (9) in a rotated frame of reference around the *y* axis by an angle β^* with respect to principal directions *x* and *z*. Values of standard deviations $\Delta\xi^*$ and $\Delta\zeta^*$ are in degrees, whereas correlation coefficients $\rho_{\xi^*\zeta^*}$, $\rho_{\xi^*\eta^*}$ and $\rho_{\eta^*\zeta^*}$ are dimensionless.

	Numerically generated surface					Statistical model		
β^*	$\Delta\xi^*$	$\Delta\zeta^*$	$\rho_{\xi^*\zeta^*}$	$\rho_{\xi^*\eta^*}$	$\rho\eta^*\zeta^*$	$\Delta\xi^*$	$\Delta\zeta^*$	$\rho_{\xi^*\zeta^*}$
0°	2.32	7.59	0.05	0.03	−0.02	2.50	7.50	0.00
30°	4.38	6.09	−0.73	0.02	0.04	4.53	6.53	−0.76
60°	6.66	4.30	−0.73	−0.06	0.00	6.53	4.53	−0.76
90°	7.67	2.45	−0.08	0.00	0.03	7.50	2.50	0.00

2.3. Statistical modelling of the vector angles ξ^* and ζ^* for any given reference frame rotation angle β^*

According to deterministic simulation results, in the frame of low roughness given by Eq. (6), we can assume that virtual normal vector angles ξ^* and ζ^* are random variables, $(\xi^*,\zeta^*) \in [0,\pi]^2$ that obey a Bivariate Normal Distribution:

$$P_{\xi^*\zeta^*}(\theta,\varphi) = \frac{1}{2\pi\sqrt{1-\rho^2_{\xi^*\zeta^*}}\,\Delta\xi^*\,\Delta\zeta^*}\exp\left[-\frac{z^2_{\xi^*\zeta^*}}{2\left(1-\rho^2_{\xi^*\zeta^*}\right)}\right], \quad (\theta,\varphi)\in[0,\pi]^2 \tag{11}$$

where

$$z^2_{\xi^*\zeta^*} \equiv \frac{\left(\theta-\mu_{\xi^*}\right)^2}{\Delta\xi^{*2}} - \frac{2\rho_{\xi^*\zeta^*}\left(\theta-\mu_{\xi^*}\right)\left(\varphi-\mu_{\zeta^*}\right)}{\sqrt{\Delta\xi^{*2}\Delta\zeta^{*2}}} + \frac{\left(\varphi-\mu_{\zeta^*}\right)^2}{\Delta\zeta^{*2}}$$

and $\rho_{\xi^*\zeta^*}$ is the correlation coefficient of angles ξ^* and ζ^* given by Eq. (8), mean values $\mu_{\xi^*} = \mu_{\zeta^*} = \pi/2$ and variances $\Delta\xi^{*2}$ and $\Delta\zeta^{*2}$ and covariance $\mathrm{Cov}(\xi^*,\zeta^*)$ follow from Eq. (9).

The marginal distributions of angles ξ^* and ζ^* then obey Normal distributions, given by,

$$P_{\xi^*}(\theta) = \frac{1}{\sqrt{2\pi\Delta\xi^{*2}}}\exp\left[\frac{-\left(\theta-\mu_{\xi^*}\right)^2}{2\Delta\xi^{*2}}\right], \quad \theta\in[0,\pi] \tag{12}$$

and

$$P_{\zeta^*}(\varphi) = \frac{1}{\sqrt{2\pi\Delta\zeta^{*2}}}\exp\left[\frac{-\left(\varphi-\mu_{\zeta^*}\right)^2}{2\Delta\zeta^{*2}}\right], \quad \varphi\in[0,\pi] \tag{13}$$

From numerical calculations, it is confirmed that angles ξ^* and ζ^* obey Normal distributions Eqs. (12) and (13), respectively, with mean values $\mu_{\xi^*} = \mu_{\zeta^*} = \pi/2$ and variances $\Delta\xi^{*2}$ and $\Delta\zeta^{*2}$ that follow from Eq. (9).

2.4. Link between anisotropic surface parameters and standard deviations of virtual wall normal vector angles

For a one-dimensional Gaussian wall roughness profile, as described by Tsang et al. [32], it holds that

$$\sigma = \sqrt{2}\,\frac{h}{c_L} \quad \text{(in radians)} \tag{14}$$

where σ is the rms of the wall roughness inclination slope, h is the rms roughness height and c_L represents the correlation length scale of that profile.

Comparison of Eq. (14) with rms of wall roughness inclination slopes along the x and z principal directions is shown in Fig. 4a and Fig. 4b, respectively. These slopes are calculated in every triangular mesh cell as $s_x = -n_x/n_y$ and $s_z = -n_z/n_y$, respectively. As can be seen, the agreement between Eq. (14) and values calculated from the generated surface is very good.

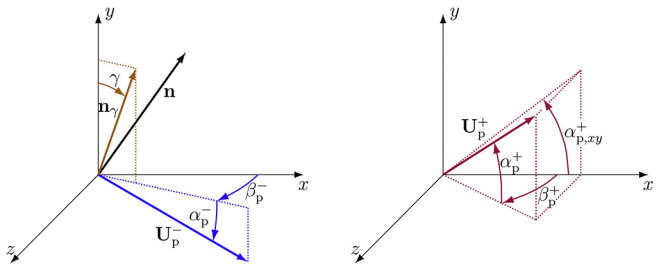

Fig. 5. Angles of particle incident velocity $\mathbf{U}_p^-$ and angles of particle rebound velocity $\mathbf{U}_p^+$. Unit virtual wall normal vectors $\mathbf{n}$ and $\mathbf{n}_\gamma$ are defined in Eqs. (3) and (17), respectively.

It can be seen from Fig. 4 that agreement of Eq. (14) and the virtual wall normal vector angle standard deviations $\Delta\xi$ and $\Delta\zeta$ calculated from the numerically generated surface is excellent in the case of low roughness given by Eq. (6). Therefore, up to approximately 0.13 rad (7.5°), it holds that,

$$\Delta\xi = \sqrt{2}\,\frac{h}{c_{Lx}} \qquad \Delta\zeta = \sqrt{2}\,\frac{h}{c_{Lz}} \tag{15}$$

3. Numerical simulation of 3D elastic bouncing of particles on an anisotropic rough wall and statistical analysis of results

3.1. Description of numerical simulation

The goal of deterministic simulations of 3D ideally elastic bouncing of particles on an anisotropic rough wall is to give the statistical properties of particle rebound angles α_p^+ and β_p^+ and of virtual wall normal vector angles ξ and ζ "seen" by the particles, for different particle incident angles α_p^- and β_p^- (Fig. 5). Particle incident angles are defined by

$$\alpha_p^- = \arcsin\left(\frac{v_p^-}{|\mathbf{U}_p^-|}\right), \quad \alpha_p^-\in[-\pi/2, 0]$$

$$\beta_p^- = -\,\mathrm{sgn}\left(w_p^-\right)\arccos\left(\frac{u_p^-}{|\mathbf{U}_p^-|\cos\left(\alpha_p^-\right)}\right), \quad \beta_p^-\in[-\pi,\pi]$$

In this section, particle rebound characteristics are calculated for two surfaces determined with virtual normal vector angle standard deviations $(\Delta\xi,\Delta\zeta) = (2.5\,^\circ, 7.5^\circ)$ and $(\Delta\xi,\Delta\zeta) = (7.5\,^\circ, 2.5^\circ)$.

The procedure of the numerical simulation can be summarized as follows. Coordinates x and z of the particle centre are sampled from a

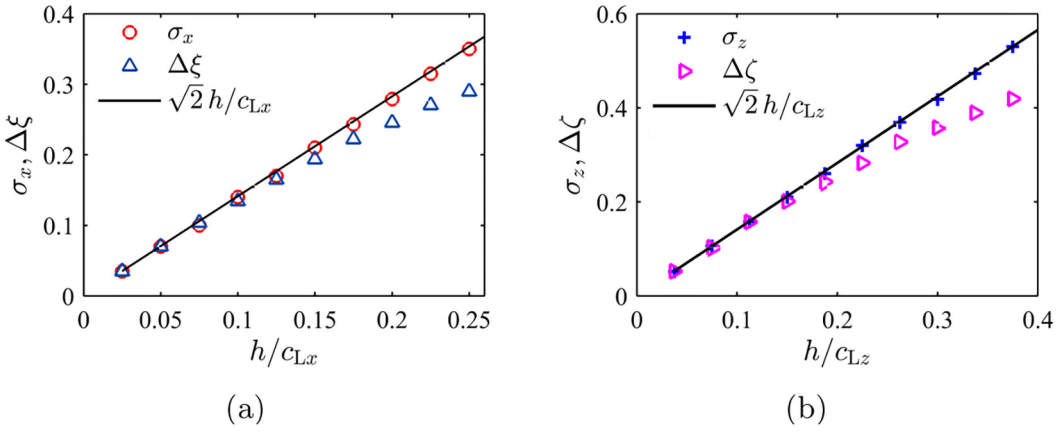

Fig. 4. Comparison of Eq. (14) with the rms of wall roughness inclination slopes and standard deviations of virtual normal vector angles $\Delta\xi$ (Fig. a) and $\Delta\zeta$ (Fig. b). Values on the abscissa are dimensionless and values on the ordinate axis are in radians.

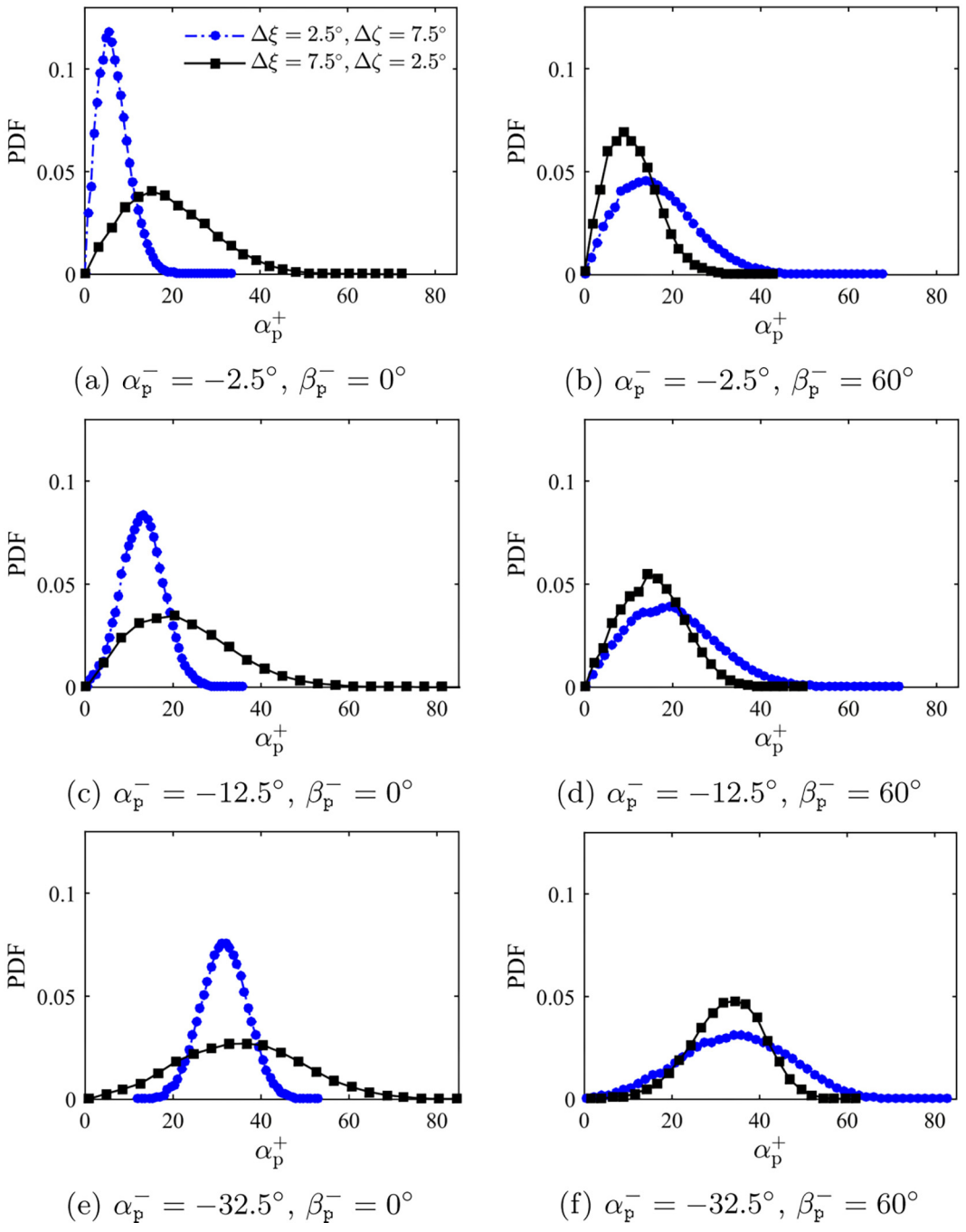

Fig. 6. PDFs of the final particle rebound angle α_p^+ before their return to the flow, computed from deterministic simulations for anisotropic walls characterized by normal vector angle standard deviations $\Delta\xi$ and $\Delta\zeta$, for particle vertical incident angle $\alpha_p^- = -2.5°$, $-12.5°$ or $-32.5°$ and transverse incident angle $\beta_p^- = 0°$ (left column) or 60° (right column). Angle α_p^+ is in degrees.

Uniform distribution, whereas the y coordinate of the particle centre is slightly higher than the highest asperity of the sampled virtual wall. Under prescribed particle incident angles, the first point of intersection of the particle centre trajectory and the virtual wall is found. At this intersection point, the global coordinate system (x,y,z) is rotated to the local coordinate system (x',y',z'), such that the virtual wall normal $\mathbf{n}$ coincides with the y' axis. Equations for the ideally elastic rebound of particles are then applied: $u'^+_p = u'^-_p$; $v'^+_p = -v'^-_p$; $w^+_p = w'^-_p$ (particle incident characteristics are denoted with superscript $^-$ and particle rebound characteristics are denoted with superscript $^+$) and subsequently the obtained rebound velocities are rewritten in the global coordinate system. The particle centre is further tracked and if the particle centre after rebound intersects the virtual wall again, i.e. there are multiple particle-wall collisions, the described procedure for the calculation of particle rebound is repeated. The particle centre is tracked until it does not pass the highest asperity in the sampled virtual wall domain.

Results of performed simulations have shown that tracking around 10,000 particle centres is sufficient to obtain converged statistics. Considering that rebound of particles from the wall is calculated as ideally elastic, the statistics obtained are independent of the value of the incident velocity norm.

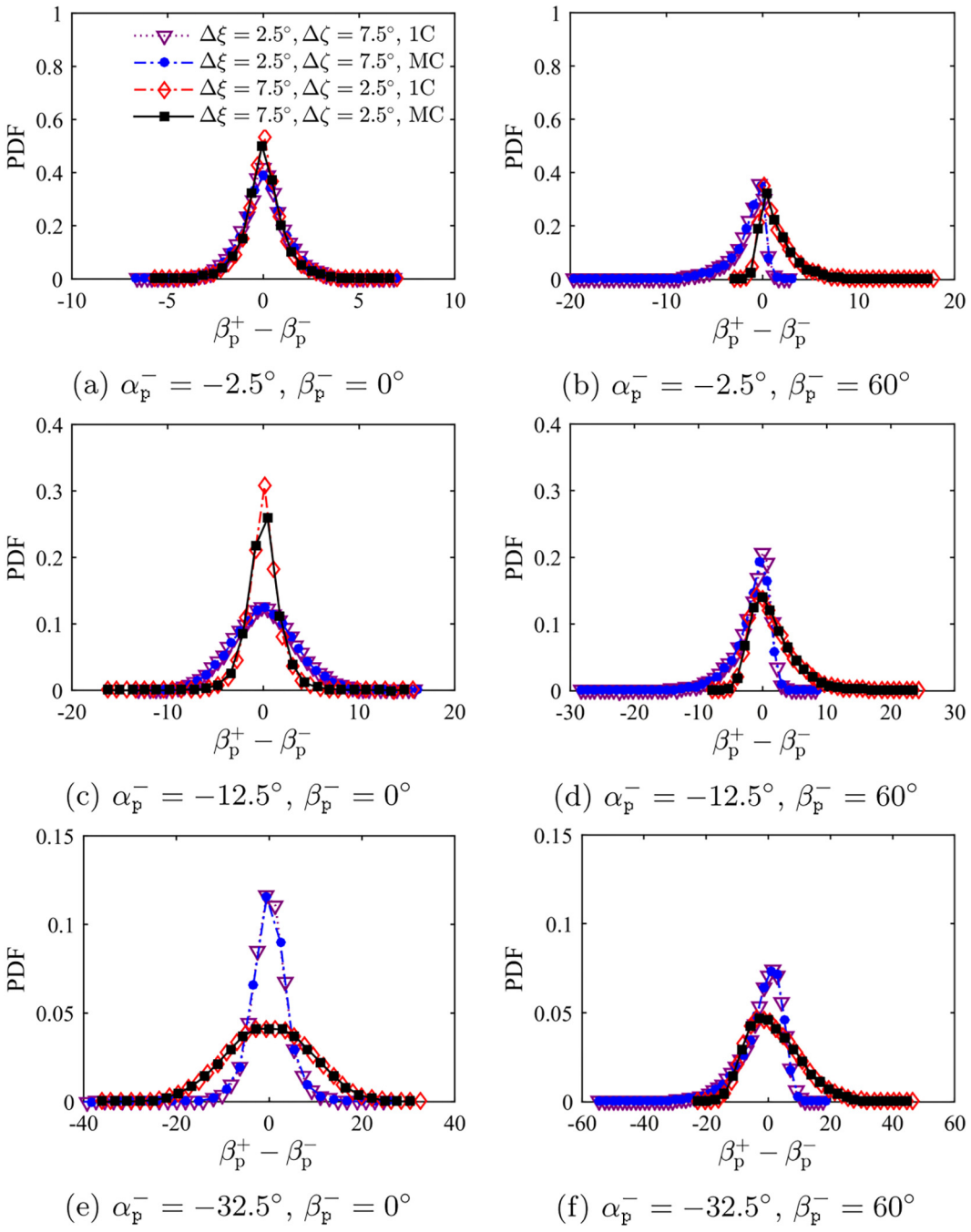

Fig. 7. PDFs of the transverse deviation angle $\beta_p^+ - \beta_p^-$ in the case of the first (1C) and the final (MC) rebound of particles from the wall before their return to the flow, computed from deterministic simulations for anisotropic walls characterized by normal vector angle standard deviations $\Delta\xi$ and $\Delta\zeta$, for particle vertical incident angle $\alpha_p^- = -2.5°$, $-12.5°$ or $-32.5°$ and transverse incident angle $\beta_p^- = 0°$ (left column) or 60° (right column). Angle $\beta_p^+ - \beta_p^-$ is in degrees.

3.2. Statistical analysis of 3D particle rebound from an anisotropic rough wall

PDFs of particle rebound angles α_p^+ for different particle incident angles α_p^- and β_p^- are shown in Fig. 6. At large particle vertical incident angles α_p^- ($|\alpha_p^-| \gg \Delta\xi$ and $\Delta\zeta$), the rebound angle α_p^+ obeys a nearly Normal distribution with a mean value equal to the absolute value of the particle vertical incident angle, $\mu_{\alpha_p^+} = |\alpha_p^-|$. As the absolute value of vertical incident angle $|\alpha_p^-|$ decreases, mean value $\mu_{\alpha_p^+}$ of particle rebound angle α_p^+ also decreases, but slower, such that at low particle vertical incident angles α_p^- (of the order of $\Delta\xi$ and $\Delta\zeta$), $\mu_{\alpha_p^+}$ becomes larger than $|\alpha_p^-|$.

This behaviour was pointed out by previous studies and is due to several effects. On one hand, by definition, the final bouncing angles of particle returning to the flow takes only positive values. So, the PDF must be truncated for α_p^+ less than zero and may not be a simple Normal distribution. On the other hand, Sommerfeld and Huber [8] show that the so-called shadow effect will modify the virtual wall normal distribution angle seen by particles with small vertical incident angles and that will change the bouncing angles statistics. Finally, Konan et al. [9] show that particles bouncing with small incident angles may undergo multiple collisions with the wall which will also change the final distribution of the bouncing angles of the particles when they return to the flow.

Fig. 7 shows PDFs of the transverse deviation bouncing angle $\beta_p^+ - \beta_p^-$ for a particle transverse incident angle β_p^- equal to 0° or 60°. For $\beta_p^- = 0°$, PDFs obey Normal distributions with zero mean and a standard deviation that increases with increase in the absolute value of the

particle vertical incident angle $|\alpha_p^-|$. This behaviour is also characteristic of the PDF of transverse deviation bouncing angle $\beta_p^+ - \beta_p^-$ in the case of particle rebound from a 3D isotropic rough wall. A stochastic model for such a rough wall was proposed by Radenkovic and Simonin [29]. For particle transverse incident angle $\beta_p^- = 60°$, PDFs of transverse deviation angles $\beta_p^+ - \beta_p^-$ are not symmetric and do not obey a Normal distribution. For these cases, the mean values of these distributions are of the order of a few degrees and the standard deviations of these distributions increase with increase in the absolute value of the particle vertical incident angle $|\alpha_p^-|$.

For all particle transverse incident angles β_p^- examined (Fig. 7), there is excellent agreement between the PDF of the transverse deviation angle after the first rebound of the particle from the wall and the PDF of the transverse deviation angle after the final rebound of the particle from the wall before its return to the flow, which suggests that the PDF of the transverse deviation angle after particle rebound from an anisotropic rough wall is not significantly influenced by multiple particle-wall collisions.

As can be seen from Fig. 7, when particles rebound from an anisotropic rough wall and the particle transverse incident angle is $\beta_p^- = 60°$, for which the particle vertical incident plane is not collinear with either of the two principal directions of roughness, after rebounding the particles are "pushed" towards the principal direction of low roughness:

- for virtual wall normal vector angle standard deviations $\Delta\xi = 2.5^\circ < \Delta\zeta = 7.5^\circ$, after rebounding from wall the particles are "pushed" towards the direction that corresponds to $\beta_p^- = 0^\circ$. In this case, the mean particle final transverse rebound angle β_p^+ before the particles return to the main flow is smaller than the particle transverse incident angle β_p^-.

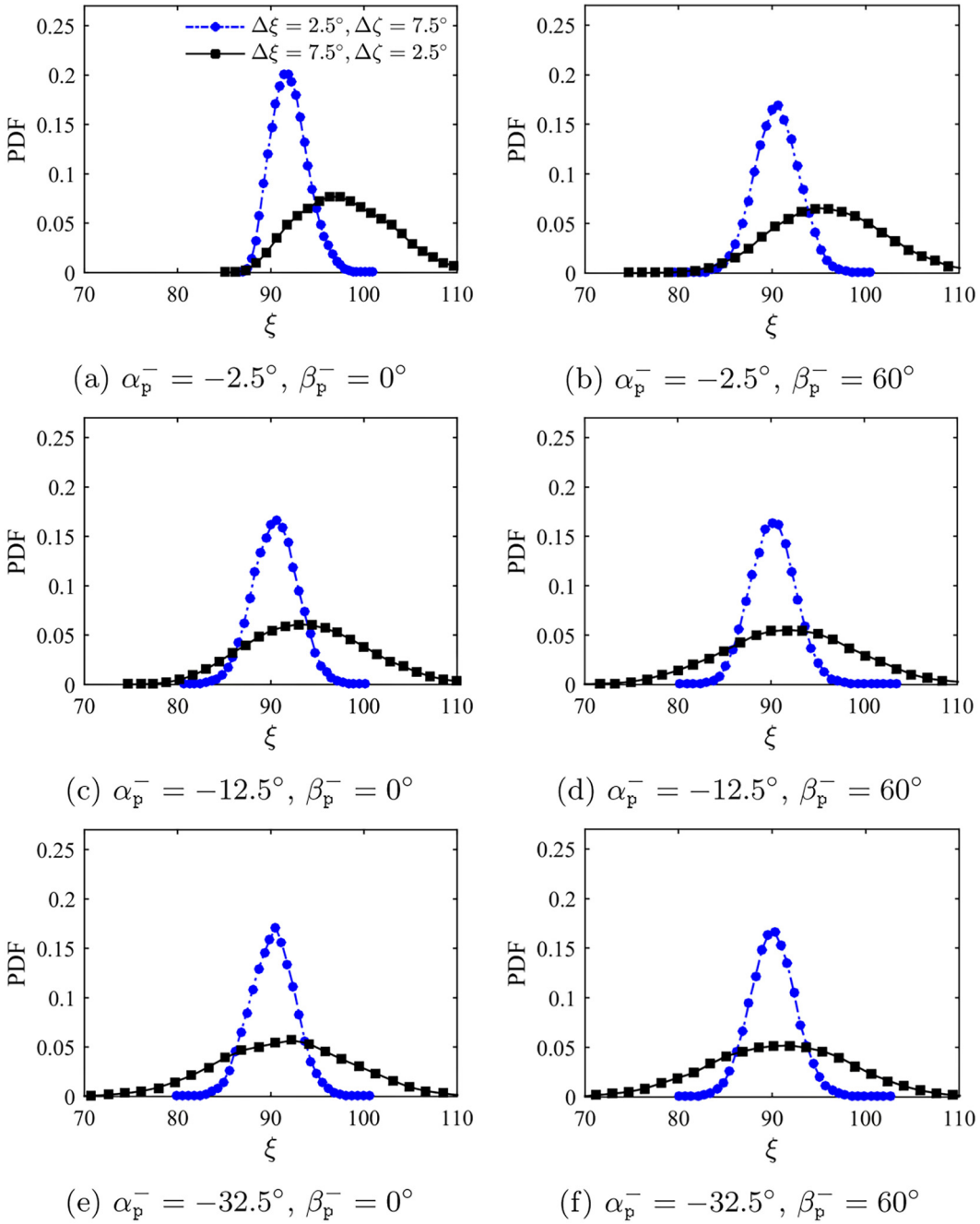

Fig. 8. PDFs of the first vector angle ξ seen by incident particles computed from deterministic simulations for anisotropic walls characterized by normal vector angle standard deviations $\Delta\xi$ and $\Delta\zeta$, for particle vertical incident angle $\alpha_p^- = -2.5°, -12.5°$ or $-32.5°$ and transverse incident angle $\beta_p^- = 0°$ (left column) or 60° (right column). Angle ξ is in degrees.

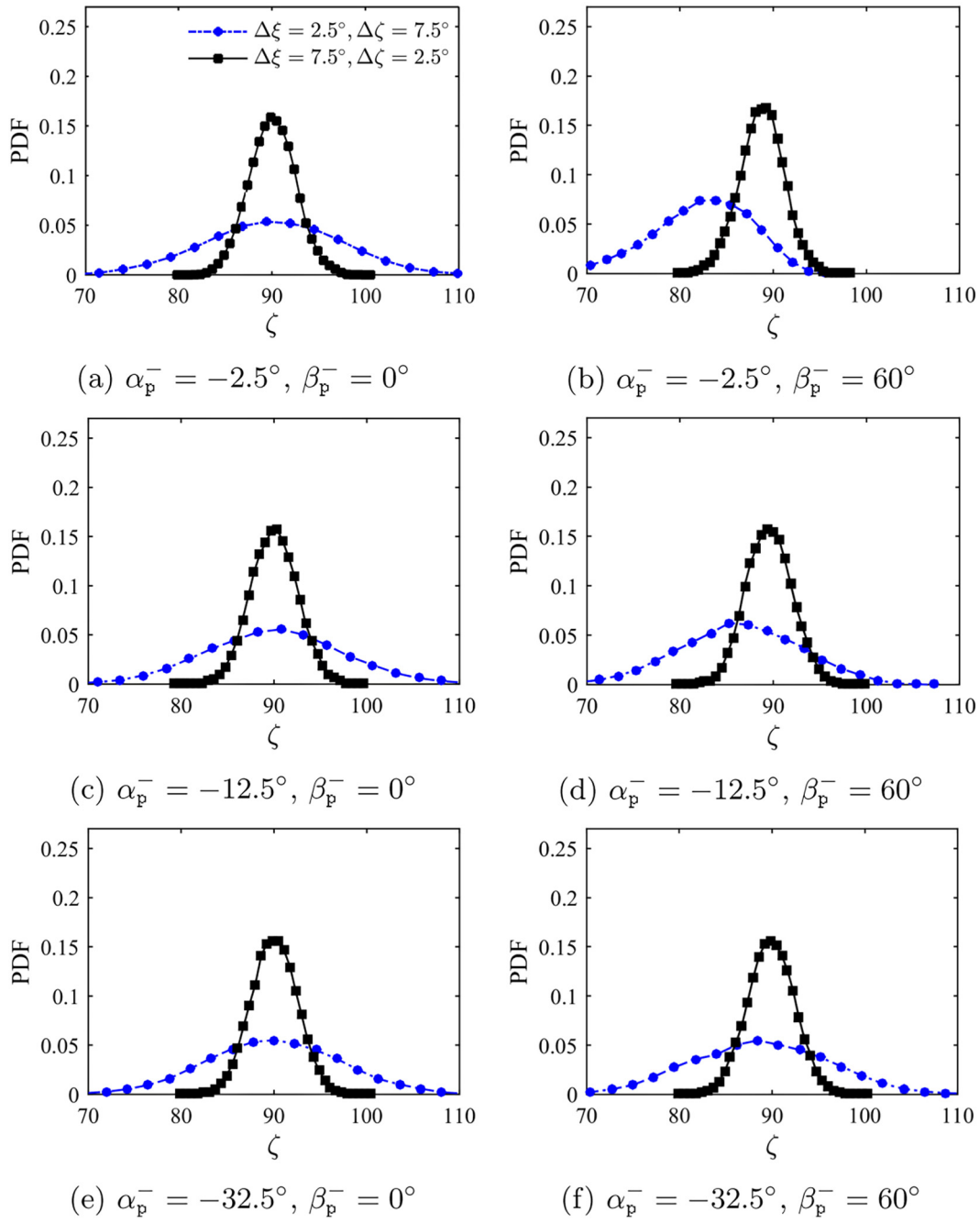

Fig. 9. PDFs of the first vector angle ζ seen by incident particles computed from deterministic simulations for anisotropic walls characterized by normal vector angle standard deviations $\Delta\xi$ and $\Delta\zeta$, for particle vertical incident angle $\alpha_p^- = -2.5°$, $-12.5°$ or $-32.5°$ and transverse incident angle $\beta_p^- = 0°$ (left column) or 60° (right column). Angle ζ is in degrees.

- for virtual wall normal vector angle standard deviations $\Delta\xi = 7.5° > \Delta\zeta = 2.5°$, after rebounding from wall the particles are "pushed" towards the direction that corresponds to $\beta_p^- = 90°$. In this case, the mean particle final transverse rebound angle β_p^+ before the particles return to the main flow is larger than the particle transverse incident angle β_p^-.

3.3. Statistical analysis of the first virtual wall normal vector "seen" by incident particles

The angles ξ and ζ of the first virtual normal vector "seen" by incident particles for different particle vertical and transverse incident angles, α_p^- and β_p^-, respectively, are shown in Figs. 8 and 9. As can be seen, at large particle vertical incident angles α_p^- ($|\alpha_p^-| \gg \Delta\xi$ and $\Delta\zeta$), angles ξ and ζ obey Normal distributions with nearly zero mean and standard deviations $\Delta\xi$ and $\Delta\zeta$ and variances Var(ξ) and Var(ζ), respectively. Such values of standard deviations $\Delta\xi$ and $\Delta\zeta$ and variances Var(ξ) and Var(ζ), are the same as ones calculated from virtual wall normal vector angles ξ and ζ, Section 2.2, Var(ξ) = $\Delta\xi^2$ and Var(ζ) = $\Delta\zeta^2$.

In contrast, as the absolute value of the particle vertical incident angle $|\alpha_p^-|$ decreases, due to the shadow effect pointed out by Sommerfeld and Huber [8], for the transverse incident angle $\beta_p^- = 0°$ the distribution of angle ξ changes whereas the distribution of angle ζ remains the same. For the transverse incident angle $\beta_p^- = 90°$ the distribution of angle ζ changes whereas the distribution of ξ remains the same and for transverse incident angles $\beta_p^- = 30°$ and 60°, the distributions of both angles ξ and ζ change shape.

The influence of the shadow effect is less pronounced for the distributions of angle ξ for a virtual wall with normal vector angle deviations $\Delta\xi = 2.5°$ and $\Delta\zeta = 7.5°$ and the distributions of angle ζ for a virtual wall with normal vector angle deviations $\Delta\xi = 7.5°$ and $\Delta\zeta = 2.5°$.

At large particle vertical incident angles α_p^- ($|\alpha_p^-| \gg \Delta\xi$ and $\Delta\zeta$), virtual wall normal vector angles ξ and ζ are random variables obeying a Bivariate Normal Distribution:

$$P_{\xi\zeta}(\theta,\varphi) = \frac{1}{2\pi\sqrt{\Delta\xi^2\Delta\zeta^2}} \exp\left[\frac{-\left(\theta-\mu_\xi\right)^2}{2\Delta\xi^2} + \frac{-\left(\varphi-\mu_\zeta\right)^2}{2\Delta\zeta^2}\right], \tag{16}$$

with $(\theta,\varphi) \in [0,\pi]^2$, mean values $\mu_\xi = \mu_\zeta = \pi/2$ and variances $\Delta\xi^2$ and $\Delta\zeta^2$, respectively.

Therefore, for these large particle vertical incident angles α_p^-, angles ξ and ζ could be directly sampled from Eq. (16). However, when the particle vertical incident angle decreases, due to the incident perspective, particles do not "see" with equal probability the lee and luv sides of roughness, and as Figs. 8 and 9 show, the distributions of angles ξ and ζ change and a specific approach needs to be developed.

3.4. Modelling the first virtual wall normal vector "seen" by particles

To account for the shadow effect in the 3D modelling of the first virtual wall normal vector seen by incident particles, Radenkovic and Simonin [29] introduce the unit normal vector $\mathbf{n}_\gamma$ (Fig. 5):

$$\mathbf{n}_\gamma = -\sin(\gamma)\mathbf{t}_p^- + \cos(\gamma)\mathbf{j}, \qquad \gamma \in \left[-\frac{\pi}{2}, \frac{\pi}{2}\right] \tag{17}$$

where $\mathbf{t}_p^-$ is the unit vector collinear with the projection of the incident particle velocity $\mathbf{U}_p^-$ on the horizontal plane:

$$\mathbf{t}_p^- = \cos\left(\beta_p^-\right)\mathbf{i} - \sin\left(\beta_p^-\right)\mathbf{k}, \qquad \beta_p^- \in [-\pi,\pi] \tag{18}$$

Then, it is imposed that the scalar projection of the unit vector $\mathbf{n}_\gamma$ onto the particle incident velocity $\mathbf{U}_p^-$ is equal to that of the unit normal vector $\mathbf{n}$,

$$\mathbf{U}_p^- \cdot \mathbf{n}_\gamma = \mathbf{U}_p^- \cdot \mathbf{n} \tag{19}$$

So, the shadow effect realisability condition for virtual wall normal vector $\mathbf{n}$ "seen" by incident particles with velocity $\mathbf{U}_p^-$, given by $\mathbf{U}_p^- \cdot \mathbf{n} < 0$ and the corresponding statistical approach developed by Sommerfeld and Huber [8] may be applied on unit vector $\mathbf{n}_\gamma$ which belongs to the particle incident plane.

In the frame of low roughness approximation, as shown by Radenkovic and Simonin [29], from the Eq. (19) follows the first order solution for the angle γ:

$$\gamma = \cos\left(\beta_p^-\right)\xi' - \sin\left(\beta_p^-\right)\zeta' \tag{20}$$

To compute virtual wall normal vector $\mathbf{n}$, the additional angle γ^* is defined in [29] as:

$$\gamma^* = \sin\left(\beta_p^-\right)\xi' + \cos\left(\beta_p^-\right)\zeta' \tag{21}$$

such that the transverse virtual wall normal vector component is written

$$\mathbf{n} - \mathbf{n}_\gamma = -\gamma^* \mathbf{s}_p \tag{22}$$

where $\mathbf{s}_p = \mathbf{t}_p^- \times \mathbf{j}$ is the unit vector orthogonal to the particle incident plane.

The angle γ^* allows accounting for the particle transverse rebound effect when the virtual wall normal vector $\mathbf{n}$ does not belong to the particle incident plane.

Angles γ and γ^*, with definitions in Eqs. (20) and (21), represent virtual wall inclination angles defined in the particle incident plane and the orthogonal plane, respectively.

Finally, the virtual normal vector angles may be computed as,

$$\begin{aligned} \xi &= \cos\left(\beta_p^-\right)\gamma + \sin\left(\beta_p^-\right)\gamma^* + \frac{\pi}{2} \\ \zeta &= -\sin\left(\beta_p^-\right)\gamma + \cos\left(\beta_p^-\right)\gamma^* + \frac{\pi}{2} \end{aligned} \tag{23}$$

Using Eqs. (3) and (23), η may be written as

$$\eta = \sqrt{\gamma^2 + \gamma^{*2}} \tag{24}$$

At large particle vertical incident angles α_p^- ($|\alpha_p^-| \gg \Delta\xi$ and $\Delta\zeta$), the shadow effect is negligible and according to Eqs. (9), (11), (20) and (21), the angles γ and γ^* are assumed to obey a Bivariate Normal Distribution:

$$P_{\gamma\gamma^*}(\theta,\varphi) = \frac{1}{2\pi\sqrt{1-\rho_{\gamma\gamma^*}^2}\,\Delta\gamma\Delta\gamma^*} \exp\left[-\frac{z_{\gamma\gamma^*}^2}{2\left(1-\rho_{\gamma\gamma^*}^2\right)}\right] \tag{25}$$

where

$$z_{\gamma\gamma^*}^2 \equiv \frac{\left(\theta-\mu_\gamma\right)^2}{\Delta\gamma^2} - \frac{2\rho_{\gamma\gamma^*}\left(\theta-\mu_\gamma\right)\left(\varphi-\mu_{\gamma^*}\right)}{\sqrt{\Delta\gamma^2\Delta\gamma^{*2}}} + \frac{\left(\varphi-\mu_{\gamma^*}\right)^2}{\Delta\gamma^{*2}}, \quad (\theta,\varphi) \in \left[-\frac{\pi}{2}, \frac{\pi}{2}\right]^2$$

the mean values of angles γ and γ^* are zero, $\mu_\gamma = \mu_{\gamma^*} = 0$, the variances and covariance are defined by

$$\begin{aligned} \Delta\gamma &= \cos^2\left(\beta_p^-\right)\Delta\xi^2 + \sin^2\left(\beta_p^-\right)\Delta\zeta^2 \\ \Delta\gamma^* &= \sin^2\left(\beta_p^-\right)\Delta\xi^2 + \cos^2\left(\beta_p^-\right)\Delta\zeta^2 \\ \mathrm{Cov}(\gamma,\gamma^*) &= \sin\left(\beta_p^-\right)\cos\left(\beta_p^-\right)\left[\Delta\xi^2 - \Delta\zeta^2\right] \end{aligned} \tag{26}$$

and $\rho_{\gamma\gamma^*}$ is the correlation coefficient of angles γ and γ^*:

$$\rho_{\gamma\gamma^*} = \frac{\mathrm{Cov}(\gamma,\gamma^*)}{\Delta\gamma\Delta\gamma^*} \tag{27}$$

At large particle vertical incident angles α_p^- ($|\alpha_p^-| \gg \Delta\xi$ and $\Delta\zeta$), the stochastic modelling of the random angles γ and γ^* obeying the distribution function Eq. (25) may be carried out according to the following process,

- Angle γ is a sample according to the Normal distribution:

$$P_\gamma(\theta) = \frac{1}{\sqrt{2\pi\Delta\gamma^2}} \exp\left[\frac{-\theta^2}{2\Delta\gamma^2}\right], \quad \theta \in \left[-\frac{\pi}{2}, \frac{\pi}{2}\right] \tag{28}$$

- Angle γ^* is a sample from the Normal distribution:

$$P_{\gamma^*}(\varphi|\theta=\gamma) = \frac{1}{\sqrt{2\pi\mathrm{Var}(\gamma^*|\theta=\gamma)}} \exp\left[-\frac{\left(\varphi-\mu_{\gamma^*|\theta=\gamma}\right)^2}{2\,\mathrm{Var}(\gamma^*|\theta=\gamma)}\right] \tag{29}$$

where

$$\begin{aligned} &\varphi \in \left[-\frac{\pi}{2}, \frac{\pi}{2}\right], \quad \mu_{\gamma^*|\theta=\gamma} = \frac{\Delta\gamma^*\rho_{\gamma\gamma^*}\gamma}{\Delta\gamma}, \\ &\mathrm{Var}(\gamma^*|\theta=\gamma) = \left(1-\rho_{\gamma\gamma^*}^2\right)\Delta\gamma^{*2} \end{aligned} \tag{30}$$

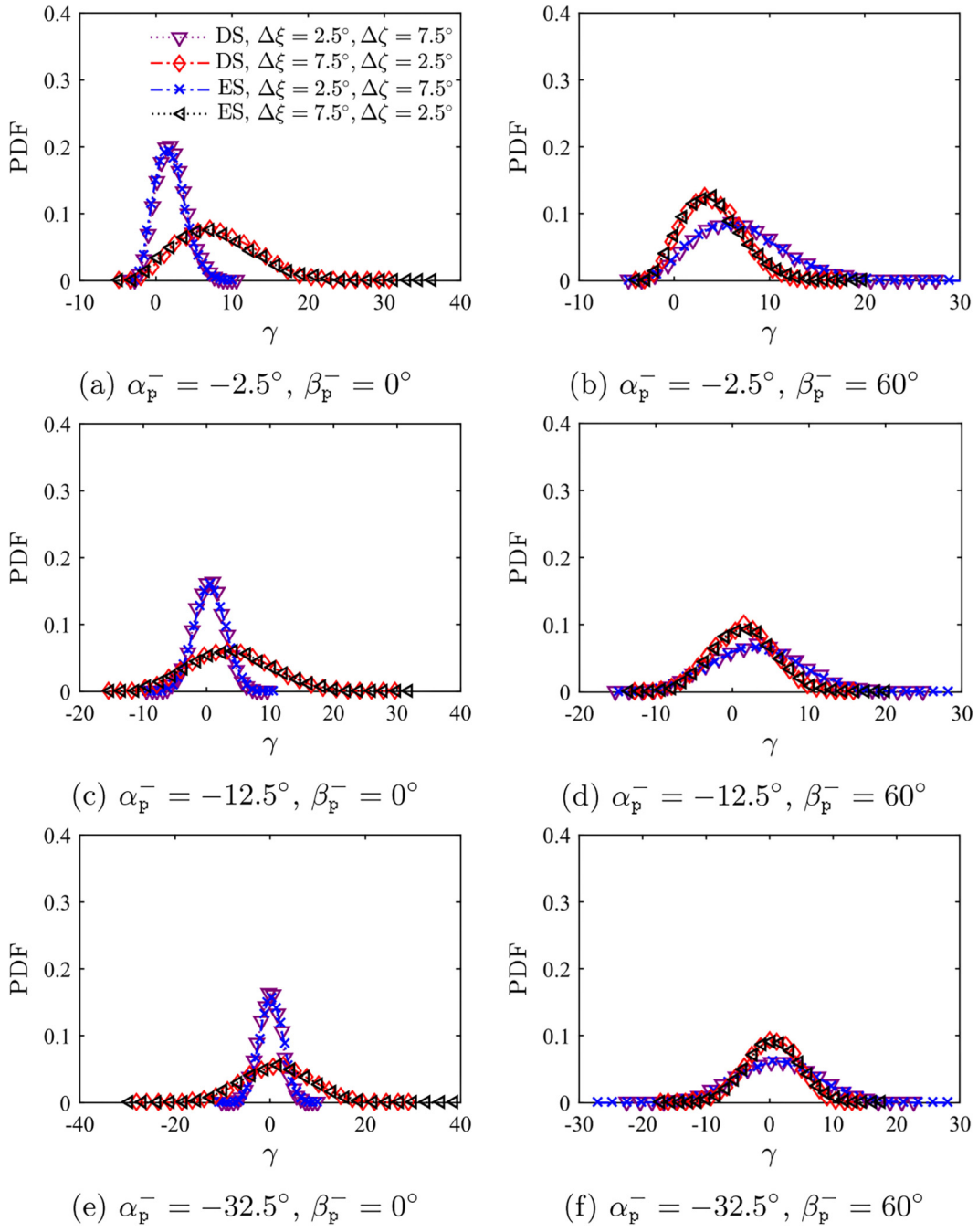

Fig. 10. PDFs of the first angle γ seen by incident particles computed from deterministic simulations (DS) for anisotropic walls characterized by normal vector angle standard deviations $\Delta\xi$ and $\Delta\zeta$ and using the effective Sommerfeld distribution (ES) given by Eqs. (31) and (32) with $\Delta\gamma$ given by Eq. (26), for particle vertical incident angle $\alpha_p^- = -2.5°, -12.5°$ or $-32.5°$ and transverse incident angle $\beta_p^- = 0°$ (left column) or 60° (right column). Angle γ is in degrees.

From Eq. (30), if $\rho_{\gamma\gamma^*} \neq 0$, then $\mu_{\gamma^*|\theta=\gamma}$ is a linear function of angle γ. Also if $\rho_{\gamma\gamma^*} \neq 0$, the variance of the conditional distribution of γ^*, given angle γ, is smaller than the variance of the marginal distribution of γ^*.

To account for the shadow effect which may become very important for small particle vertical incident angles α_p^- (of the order of $\Delta\xi$ and $\Delta\zeta$), we extend the 3D isotropic approach proposed by Radenkovic and Simonin [29] assuming that the angle γ is obeying an effective distribution given by Sommerfeld and Huber [8] conditioned by the particle vertical incident angle α_p^-:

if $\gamma \leq \alpha_p^-$:

$$P_{eff}\left(\gamma|\alpha_p^-\right) = 0 \tag{31}$$

if $\gamma > \alpha_p^-$:

$$P_{eff}\left(\gamma|\alpha_p^-\right) = \frac{1}{\sqrt{2\pi\Delta\gamma^2}} \frac{\sin\left(\alpha_p^- - \gamma\right)}{\sin\left(\alpha_p^-\right)} \exp\left(-\frac{\gamma^2}{2\Delta\gamma^2}\right) g\left(\alpha_p^-, \Delta\gamma\right) \tag{32}$$

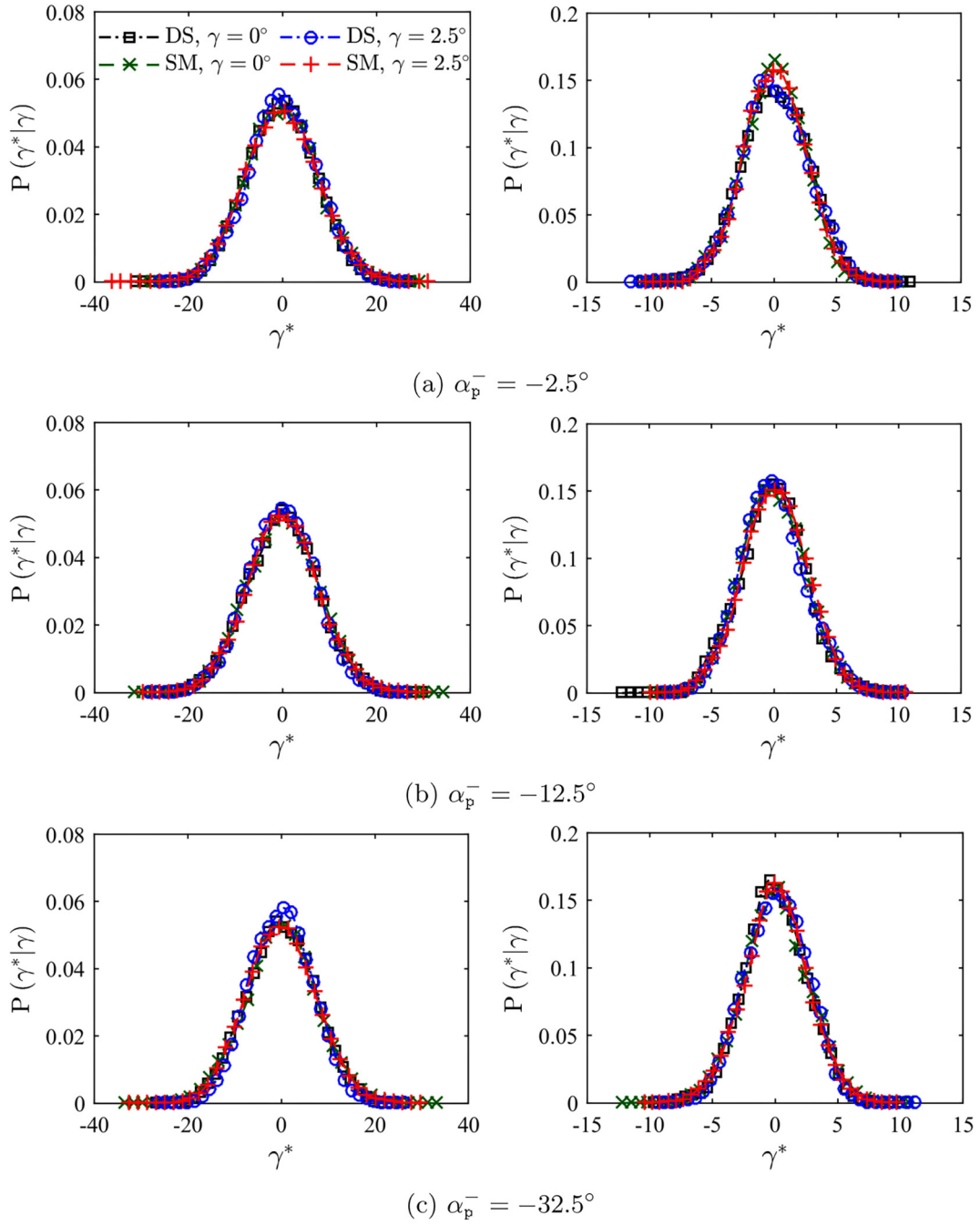

Fig. 11. PDFs of the first angle γ^* seen by incident particles, conditioned by the angle γ. PDFs are computed from deterministic simulations (DS) and using statistical model (SM) given by Eq. (29) for anisotropic walls characterized by normal vector angle standard deviations $\Delta\xi = 2.5°$ and $\Delta\zeta = 7.5°$ (left column) and $\Delta\xi = 7.5°$ and $\Delta\zeta = 2.5°$ (right column), for particle vertical incident angle $\alpha_p^- = -2.5°$, $-12.5°$ or $-32.5°$ and transverse incident angle $\beta_p^- = 0°$. Angle γ^* is in degrees.

with

$$g\left(\alpha_p^-, \Delta\gamma\right) = 1/\int_{\alpha_p^-}^{\pi/2} \frac{1}{\sqrt{2\pi\Delta\gamma^2}} \frac{\sin\left(\alpha_p^- - \gamma\right)}{\sin\left(\alpha_p^-\right)} \exp\left(-\frac{\gamma^2}{2\Delta\gamma^2}\right) d\gamma \quad (33)$$

where $\Delta\gamma$ follows from Eq. (26).

The angle γ^* is obeying the distribution given by Eq. (29), conditioned by the angle γ.

Verification of the proposed statistical model, given by Eqs. (29), (31) and (32), is shown in Figs. 10, and 11.

PDFs of the first angle γ computed with deterministic simulation and the effective Sommerfeld distribution Eqs. (31) and (32), for different particle incident angles α_p^- and β_p^- are shown in Fig. 10. The agreement between the PDFs shown is very good for all particle incident angles. It can be seen that at large particle vertical incident angles α_p^- ($|\alpha_p^-| \gg \Delta\xi$ and $\Delta\zeta$), angle γ obeys a Normal distribution with variance $\mathrm{Var}(\gamma) = \Delta\gamma^2$ given by Eq. (26). As the absolute value of angle α_p^- decreases, the distribution of angle γ is modified owing to the shadow effect.

For incident particles in a vertical plane aligned with one of the principal directions of anisotropic rough surface, $\beta_p^- \in \{0°, 90°\}$ (or in opposite directions $\beta_p^- \in \{-90°, 180°\}$) or in the case of isotropic rough surface, the proposed assumption concerning the conditional distribution of γ^* according to γ leads to an effective PDF of γ^* which is not depending on α_p^- and is simply the zero mean Normal distribution with

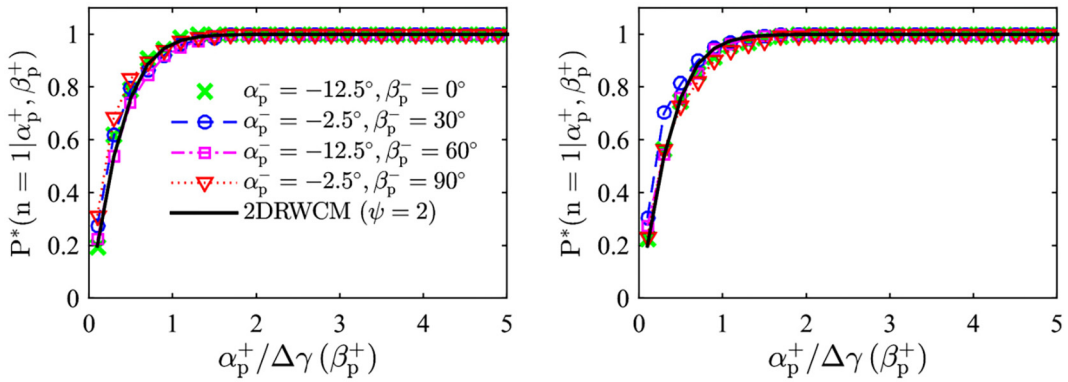

Fig. 12. Probability that particles with bouncing angle α_p^+ experience only one particle-wall collision computed from deterministic simulations and using the analytical model 2DRWCM given by Eq. (34) from Konan et al. [9] with $\psi = 2$ and $\Delta\gamma(\beta_p^+)$ computed from Eq. (35). Deterministic simulations are carried out for different particle incident angles α_p^- and β_p^- and for two different anisotropic roughness distributions characterized by the virtual normal angle standard deviations $\Delta\xi$ and $\Delta\zeta$.

variance $\mathrm{Var}(\gamma^*) = \Delta\gamma^{*2}$ given by Eq. (26). This result is confirmed in Fig. 11 showing the PDF of γ^* conditioned by the angle γ, computed from the deterministic simulation and statistical model Eq. (29) with different particle incident angles α_p^- and $\beta_p^- = 0°$ or 60°.

Therefore, for any particle vertical incident angle α_p^-, the stochastic modelling of the random angles γ and γ^* may be carried out according to the following process:

- Angle γ is sampled according to the effective Sommerfeld distribution given by Eqs. (31) and (32), with $\Delta\gamma$ that follows from Eq. (26).
- Angle γ^* is sampled according to the Normal Distribution Eq. (29). This PDF is not modified by the shadow effect.

In practical calculation, the rejection method can be used for sampling from Eq. (32).

3.5. Modelling of multiple particle collisions with the virtual wall

Multiple particle-wall collisions may significantly change the statistics of near-wall particles and a large accumulation of particles in the near-wall viscous sublayer can exist if such an effect is not accounted for [28].

According to Konan et al. [9] and Radenkovic and Simonin [29], from the deterministic simulation with 2D rough wall and 3D isotropic rough wall, respectively, the PDF of bouncing particles which undergo multiple particle-wall collisions is nearly the same as the ones that undergo only one collision, so the stochastic procedure may compute selectively bouncing particles that undergo only one collision.

As reported by Konan et al. [9], the probability of particles to undergo only one collision calculated from the deterministic simulation is given by the following analytical form:

$$P^*\left(n=1|\alpha_p^+\right) = \begin{cases} \tanh\left(\psi\dfrac{\alpha_p^+}{\Delta\gamma}\right) & \text{if } \alpha_p^+ \geq 0 \\ 0 & \text{if } \alpha_p^+ < 0 \end{cases} \tag{34}$$

where $\psi = 1.5$ and $\Delta\gamma$ is the standard deviation of virtual wall inclination angle.

Radenkovic and Simonin [29] found that Eq. (34) may also be used for modelling multiple collision effects of the 3D particle rebound from an isotropic rough wall with $\Delta\gamma = \Delta\xi = \Delta\zeta$. Such an approach may be extended directly to the anisotropic rough wall by computing the probability of only one rebound using Eq. (34) with $\Delta\gamma$ measured in the plane of the first particle rebound. In a manner similar to the derivation of Eq. (26), we may write:

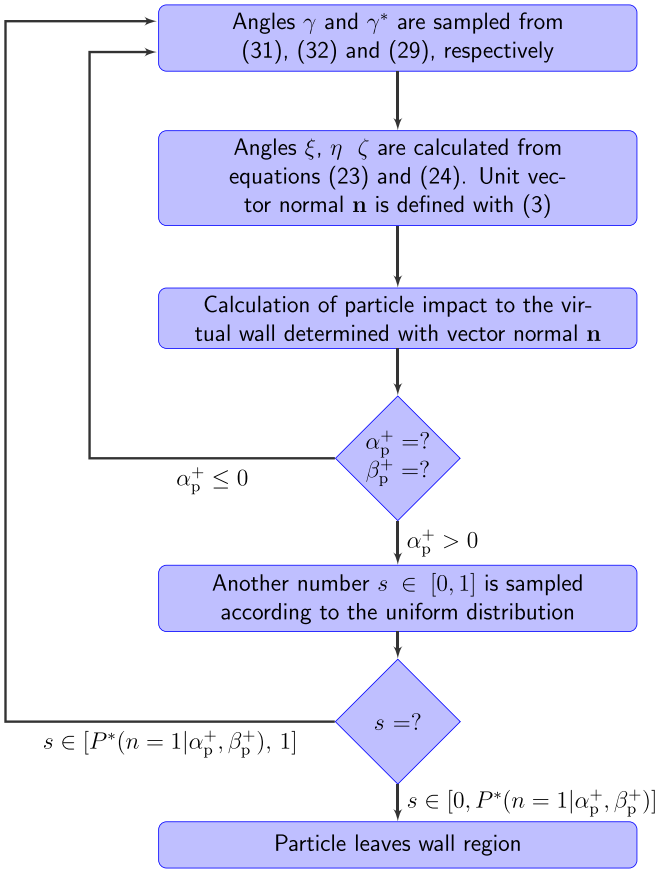

Fig. 13. Stochastic procedure for calculation of the 3D rebound of a particle from an anisotropic rough wall in a Lagrangian framework.

$$\Delta\gamma\left(\beta_p^+\right) = \sqrt{\cos^2\left(\beta_p^+\right)\Delta\xi^2 + \sin^2\left(\beta_p^+\right)\Delta\zeta^2} \tag{35}$$

In contrast to the probability of only one rebound from the isotropic rough wall, which does not depend on the particle transverse rebound angle β_p^+, the probability of only one rebound from the anisotropic wall depends on the angle β_p^+ through Eq. (35).

Fig. 12 shows a comparison of the probability Eq. (34), with $\psi = 2$ and $\Delta\gamma$ calculated from Eq. (35), that particles undergo only one particle-wall collision with the probability calculated from the deterministic simulation of the impact of particles on anisotropic surfaces with different degrees of roughness and different particle incident angles α_p^- and β_p^-. As can be seen, the agreement is very good. The value $\psi = 2$ resulted in better agreement with the results of deterministic simulations than the original value $\psi = 1.5$ used by Konan et al. [9]. This difference in agreement due to different values of ψ is a consequence of the different virtual wall generators used in the present work and by Konan et al. [9].

3.6. Stochastic procedure for calculation of the 3D rebound of a particle from an anisotropic rough wall with low roughness in a Lagrangian framework

In a Lagrangian framework, the motion of particles is governed by forces that act on a particle and to account for the particle rebound from an anisotropic rough wall, when the particle surface reaches a macroscopic smooth plane wall boundary, a stochastic procedure as shown in Fig. 13 should be applied. This procedure is a direct extension of a stochastic procedure proposed by Radenkovic and Simonin [29] for the rebound of particles from an isotropic rough wall.

4. Applications

In this section, the rebound of spherical glass particles of diameter $D_p = 500\mu$m from a rough wall made of steel, which is an experimental case reported by Sommerfeld and Huber [8], is analysed. In the frame of particle-wall collision modelling, this combination of particle size and real wall structure is equivalent to the virtual wall normal vector angle standard deviation in the main flow direction $\Delta\xi = 3.8°$.

In all numerical simulations for which results are presented in this section, the particle linear velocity in the particle incident plane is defined also according to [8]: the particle horizontal incident velocity projection u_p^- obeys a Normal distribution with mean value 5.91 m/s and standard deviation 1.16 m/s. In order to isolate the influence of anisotropic roughness on particle bouncing transverse deviation angles, the particle incident rotation is neglected.

Particle collisions with a rough wall are inelastic, with friction: the restitution coefficient and coefficient of wall friction depend on the particle vertical incident angle and they are defined as in [8]:

$$e_w\left(\alpha_p^-\right) = \begin{cases} \dfrac{e_h - 1}{\alpha_e}|\alpha_p^-| + 1 & \text{if } |\alpha_p^-| \in [0, \alpha_e] \\ e_h & \text{if } |\alpha_p^-| > \alpha_e \end{cases} \tag{36}$$

and

$$\mu_w\left(\alpha_p^-\right) = \begin{cases} \dfrac{\mu_h - \mu_0}{\alpha_\mu}|\alpha_p^-| + \mu_0 & \text{if } |\alpha_p^-| \in [0, \alpha_e] \\ e_h & \text{if } |\alpha_p^-| > \alpha_e \end{cases} \tag{37}$$

If the following condition holds:

$$v_p^- < \frac{-2}{7\mu_w(1+e_w)}|\mathbf{U}| \tag{38}$$

where the intensity of the velocity $|\mathbf{U}|$ between the particle and the wall at the contact point is

$$|\mathbf{U}| = \sqrt{\left(u_p^- + \frac{D_p}{2}\omega_{pz}^-\right)^2 + \left(w_p^- - \frac{D_p}{2}\omega_{px}^-\right)^2} \tag{39}$$

a non-sliding particle-wall collision is calculated with the equations

$$\begin{aligned} u_p^+ &= \frac{5}{7}\left(u_x^- - \frac{D_p}{5}\omega_{pz}^-\right) & \omega_{px}^+ &= \frac{2w_p^-}{D_p} \\ v_p^+ &= -e_w v_p^- & \omega_{py}^+ &= \omega_{py}^- \\ w_p^+ &= \frac{5}{7}\left(w_p^- + \frac{D_p}{5}\omega_{px}^-\right) & \omega_{pz}^+ &= -\frac{2u_p^-}{D_p} \end{aligned} \tag{40}$$

If the condition from Eq. (38) is not fulfilled, a sliding collision of a spherical particle with the wall is calculated with the equations

$$\begin{aligned} u_p^+ &= u_p^- + \varepsilon_x\mu_w(1+e_w)v_p^- & \omega_{px}^+ &= \omega_{px}^- - 5\varepsilon_z\mu_w(1+e_w)\frac{v_p^-}{D_p} \\ v_p^+ &= -e_w v_p^- & \omega_{py}^+ &= \omega_{py}^- \\ w_p^+ &= w_p^- + \varepsilon_z\mu_w(1+e_w)v_p^- & \omega_{pz}^+ &= \omega_{pz}^- + 5\varepsilon_x\mu_w(1+e_w)\frac{v_p^-}{D_p} \end{aligned} \tag{41}$$

where ε_x and ε_z are given by

$$\varepsilon_x = \frac{1}{|\mathbf{U}|}\left(u_p^- + \frac{D_p}{2}\omega_{pz}^-\right) \quad \text{and} \quad \varepsilon_z = \frac{1}{|\mathbf{U}|}\left(w_p^- - \frac{D_p}{2}\omega_{px}^-\right) \tag{42}$$

Other experimental details can be found in [8].

Deterministic and stochastic simulations of the impact of particles on a rough wall are carried out for virtual wall normal vector angle standard deviation $\Delta\xi = 3.8°$ while the standard deviation $\Delta\zeta$ is varied, so that different virtual walls are examined:

- $\Delta\zeta = 0°$ for 2D roughness,
- $\Delta\zeta = 3.8°$ for isotropic roughness and
- $\Delta\zeta = 7.5°$ for roughness with high anisotropy ($\Delta\xi < \Delta\zeta$).

The present stochastic model (SM) reduces to the 2D multiple particle-wall collision model of Konan et al. [9] if the correlation length scale in the z direction is significantly larger than that in the x direction ($c_{L,z} \gg c_{L,x}$) and to the 3D stochastic model of Radenkovic and Simonin [29] if the correlation length scales in the x and z directions are the same, $c_{L,z} = c_{L,x}$.

In this section, particle rebound characteristics are examined using deterministic and stochastic simulations for different types of roughness and for different particle vertical incident angles α_p^- and particle transverse incident angle $\beta_p^- = 0°$. Particle rebound characteristics are also analysed for different particle vertical incident angles α_p^- and particle transverse incident angle $\beta_p^- = 60°$. Finally, the mean (expected) value and standard deviation of the generated particle rebound transverse deviation angles, $E(\beta_p^+ - \beta_p^-)$ and $\Delta\beta_p^+$, respectively, are analysed for anisotropic surfaces, for different particle incident angles α_p^- and β_p^-.

10,000 particle impacts on a virtual rough wall are sufficient to obtain converged statistics.

4.1. PDFs of particle rebound angles for particle transverse incident angles $\beta_p^- = 0°$ or $\beta_p^- = 60°$

The particle rebound angle $\alpha_{p,xy}^+$ in the $x - y$ plane (Fig. 5) is linked to the rebound angle α_p^+ according to

$$\alpha_{p,xy}^+ = \arctan\left(\frac{\tan\left(\alpha_p^+\right)}{\cos\left(\beta_p^+\right)}\right) \tag{43}$$

In Fig. 14, for three different types of roughness (2D, isotropic and roughness with high anisotropy), particle rebound angles obtained

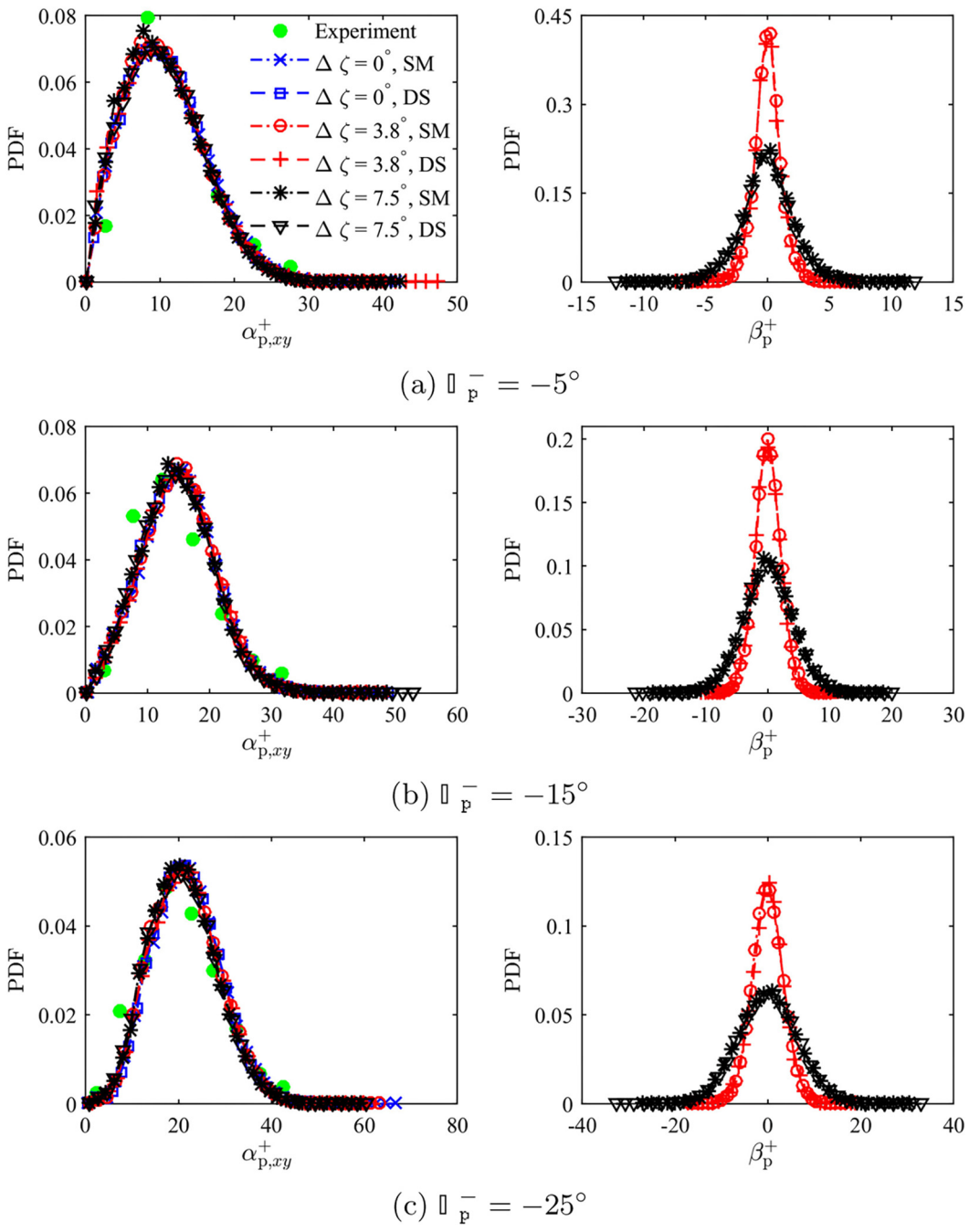

Fig. 14. PDFs of rebound angles $\alpha^+_{p,\,xy}$ and β^+_p, computed using deterministic simulation (DS) and using the stochastic model (SM). Spherical glass particles of diameter $D_p = 500\mu$m rebound from a steel wall for particle vertical incident angle $\alpha_p^- = -5°$, $-15°$ or $-25°$ and transverse incident angle $\beta_p^- = 0°$. Three different types of rough walls are examined: 2D ($\Delta\xi = 0$), isotropic ($\Delta\zeta = \Delta\xi$) and strongly anisotropic roughness ($\Delta\zeta \approx 2\Delta\xi$) with the standard deviation of virtual wall normal vector angle $\Delta\xi = 3.8°$. Experimental values are from Sommerfeld and Huber [8]. Angles $\alpha^+_{p,\,xy}$ and β^+_p are in degrees.

from numerical simulations are compared with experimental measurements of Sommerfeld and Huber [8], whereas in the $y-z$ plane only results of deterministic and stochastic simulations are compared because experimental results are not available in this plane. It can be seen that the standard deviation of the virtual wall normal vector angle $\Delta\zeta$ has a weak influence on the PDF of the particle rebound angle $\alpha^+_{p,\,xy}$, when the particle transverse incident angle is $\beta_p^- = 0°$. In the $y-z$ plane, the transverse rebound angle β^+_p obeys a Normal distribution with a standard deviation that increases with increase in the absolute value of the incident angle $|\alpha_p^-|$. For 2D roughness, the standard deviation of angle β^+_p is approximately zero for all vertical incident angles α_p^- (not shown in Fig. 14).

When the particle transverse incident angle is $\beta_p^- = 60°$, the effects of the virtual normal vector angle standard deviation $\Delta\zeta$ on the particle rebound angle α^+_p are large, as can be seen in Fig. 15. The PDF of the transverse deviation angle $\beta^+_p - \beta_p^-$ is not symmetric as in the case of particle rebound from an anisotropic surface for particle transverse angle $\beta_p^- = 0°$ or in the case of particle rebound from an isotropic surface at any particle transverse angle β_p^-.

The agreement between deterministic simulation and the stochastic model is very good in all numerical simulations. Also, the agreement between numerical simulations and the available experimental results is good.

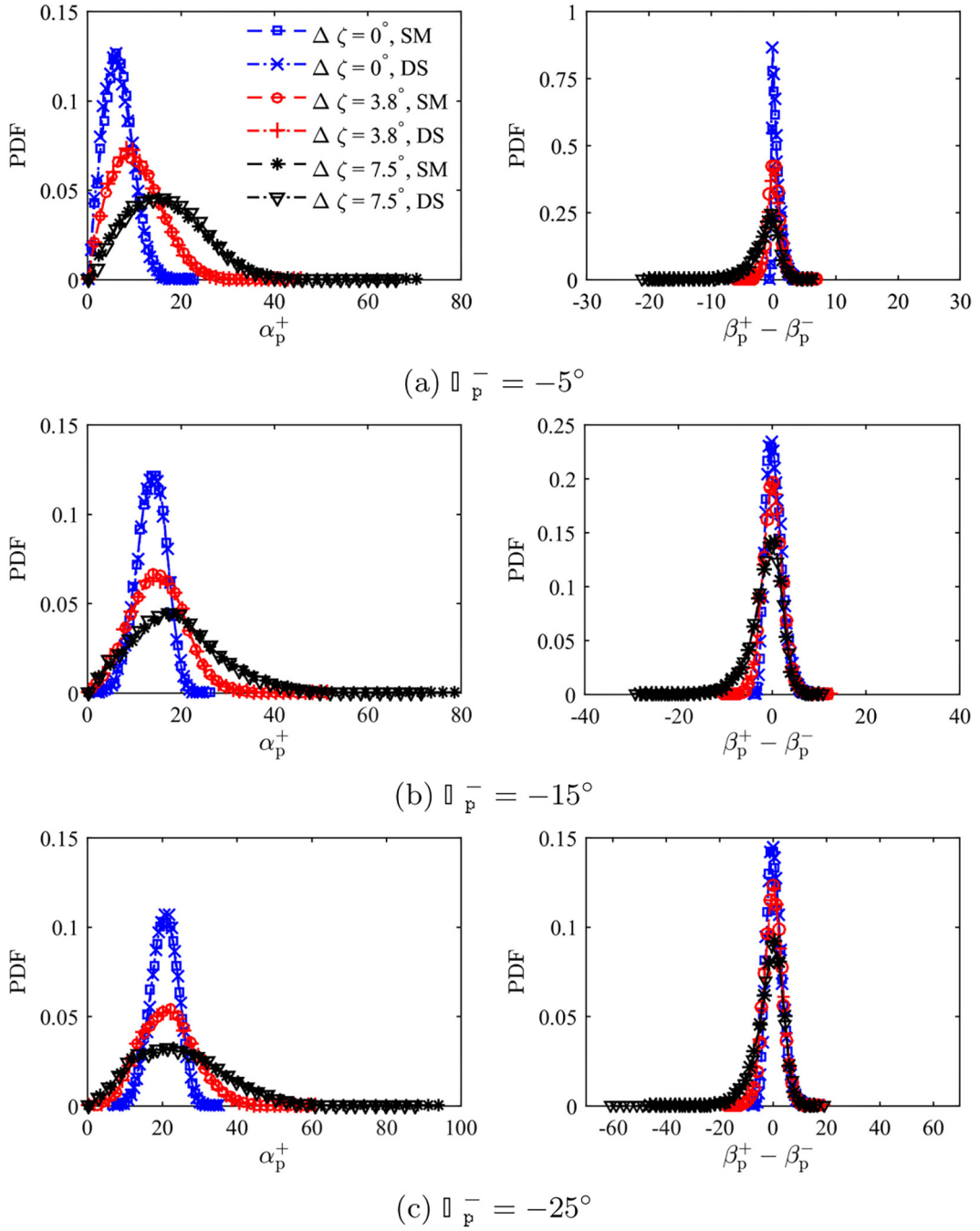

Fig. 15. PDFs of rebound angles α_p^+ (left column) and transverse deviation angle $\beta_p^+ - \beta_p^-$ (right column), computed using deterministic simulation (DS) and using the stochastic model (SM). Spherical glass particles of diameter $D_p = 500\mu$m rebound from a steel wall for particle vertical incident angle $\alpha_p^- = -5°$, $-15°$ or $-25°$ and transverse incident angle $\beta_p^- = 60°$. Three different types of rough walls are examined: 2D ($\Delta\xi = 0°$), isotropic ($\Delta\zeta = \Delta\xi$) and strongly anisotropic roughness ($\Delta\zeta \approx 2\Delta\xi$) with the standard deviation of virtual wall normal vector angle $\Delta\xi = 3.8°$. Angles α_p^+ and $\beta_p^+ - \beta_p^-$ are in degrees.

4.2. Mean value and standard deviation of the particle transverse deviation angle for particle rebound from an anisotropic rough wall, for different particle incident angles α_p^- and β_p^-

Fig. 16 shows the mean value and standard deviation of the generated particle transverse deviation angle, $E(\beta_p^+ - \beta_p^-)$ and $\Delta\beta_p^+$, respectively, in terms of particle transverse incident angle $\beta_p^- \in [0°,90°]$ and particle vertical incident angle $\alpha_p^- = -15°$, $-25°$ or $-45°$, for a wall with 2D roughness (with standard deviations of virtual wall normal vector angles $\Delta\xi = 3.8°$ and $\Delta\zeta = 0°$) and a wall with high roughness anisotropy (with standard deviations of virtual wall normal vector angles $\Delta\xi = 3.8°$ and $\Delta\zeta = 7.5°$).

It can be seen, that for both types of roughness, if the particle vertical incident plane is collinear with one of the two principal directions of roughness, the mean value of the particle transverse deviation angle E $(\beta_p^+ - \beta_p^-)$ is zero.

Although the examined particle collisions with a rough wall are inelastic, with friction, if the particle vertical incident plane is not collinear with one of two principal directions of roughness, then particles in translation rebound towards the principal direction of low roughness, as described at the end of Section 3.2 for the case of ideally elastic particle collisions with a rough wall: the mean transverse deviation angle is positive for 2D roughness (particles are "pushed" towards the principal of low roughness collinear with the *z*-axis) and negative for high

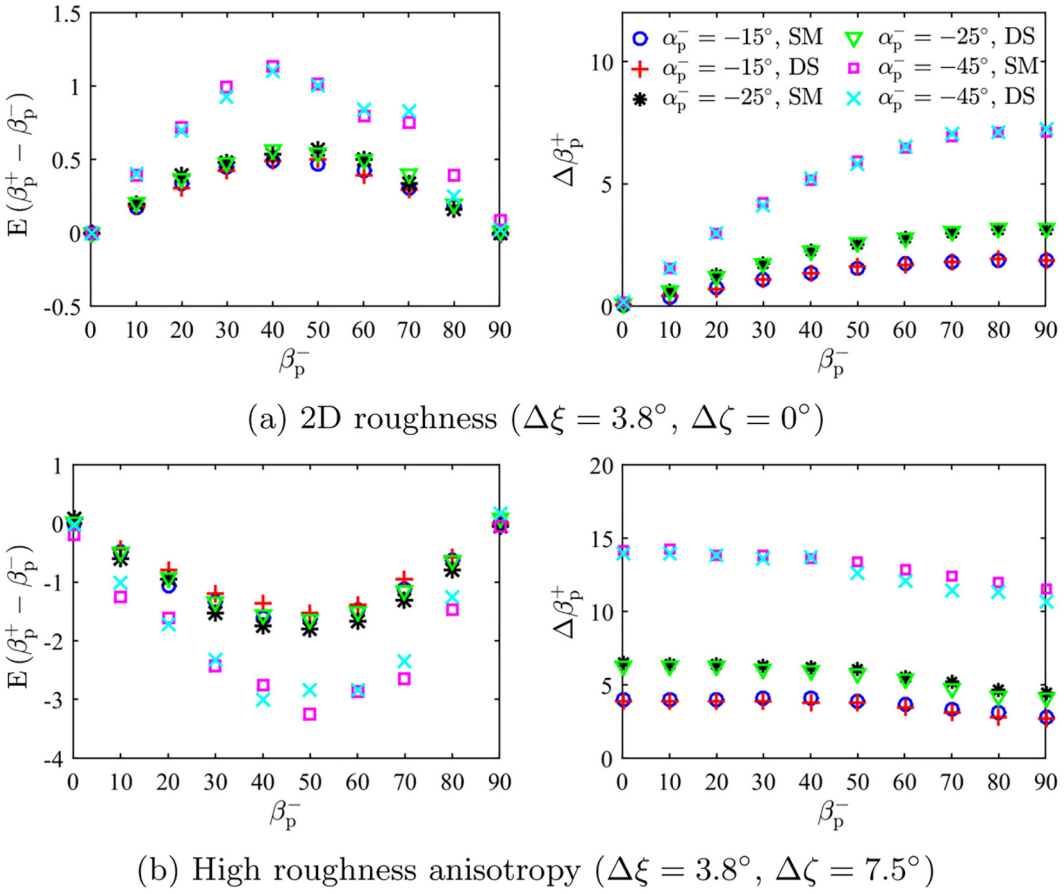

Fig. 16. Dependence of the mean value and standard deviation of the particle transverse deviation angle, $\mathrm{E}(\beta_p^+ - \beta_p^-)$ and $\Delta\beta_p^+$, respectively, on the particle transverse incident angle β_p^-, for particle vertical incident angles $\alpha_p^- = -15°$, $-25°$ or $-45°$. DS denotes results from deterministic simulation and SM denotes results from the application of the stochastic model. Spherical glass particles of diameter $D_p = 500\mu$m rebound from a steel wall with virtual wall normal vector standard deviations $\Delta\xi = 3.8°$ and $\Delta\zeta = 0°$ for 2D roughness and $\Delta\zeta = 7.5°$ for high roughness anisotropy. Values on the axes are in degrees.

roughness anisotropy (particles are "pushed" towards the principal direction of low roughness collinear with the x-axis). The magnitude of the mean value of the particle transverse deviation angle $\mathrm{E}(\beta_p^+ - \beta_p^-)$ increases with increase in the absolute value of the particle vertical incident angle $|\alpha_p^-|$.

For particle vertical incident angle $\alpha_p^- \in [-45°, 0°]$ and with the particle vertical incident plane non-collinear with one of the two principal directions of roughness, a particle after rebound from an anisotropic surface has a small magnitude of the mean transverse deviation angle, of the order of a few degrees. This effect could be important if one of the two principal directions of roughness is not collinear with the mean gas flow direction. Then, since the transverse deviation effect occurs for every bounce of the particle from the wall, the particle flow transverse angle could become significant with respect to the mean gas flow direction. The influence of this effect on particle-laden flows depends on many parameters, such as particle and flow properties,

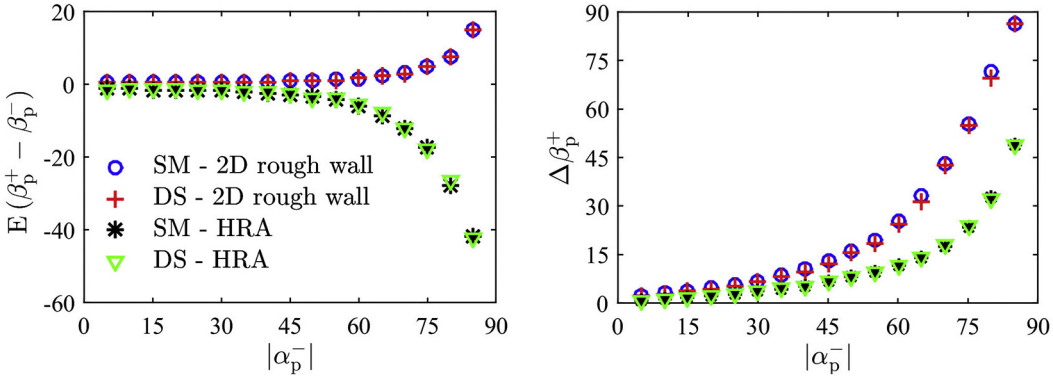

Fig. 17. Influence of the absolute value of the particle vertical incident angle $|\alpha_p^-|$ for a given transverse angle $\beta_p^- = 60°$ on the mean value and standard deviation of the particle transverse deviation angle, $\mathrm{E}(\beta_p^+ - \beta_p^-)$ and $\Delta\beta_p^+$, respectively. DS denotes deterministic simulation and SM denotes the stochastic model. Spherical glass particles of diameter $D_p = 500\mu$m rebound from a steel wall with virtual wall normal vector standard deviations $\Delta\xi = 3.8°$ and $\Delta\zeta = 0°$ for a 2D rough wall and $\Delta\zeta = 7.5°$ for a wall with high roughness anisotropy (HRA). Values on the axes are in degrees.

particle-wall collision frequency, inter-particle collisions, particle incident angles etc.

For both virtual rough walls examined (2D roughness and high roughness anisotropy), the magnitude of the mean transverse deviation angle $E(\beta_p^+ - \beta_p^-)$, for given particle vertical incident angle α_p^-, depends on the particle transverse incident angle β_p^-: for $\beta_p^- \in [0°,50°]$ the magnitude of the mean transverse deviation angle increases, whereas further increase of β_p^- (up to 90°) leads to a decrease of this magnitude.

For 2D roughness, the standard deviation of the particle transverse deviation angle $\Delta\beta_p^+$ increases with increase in the transverse incident angle β_p^-. In contrast, for a virtual wall with high roughness anisotropy there is a weak dependence of the standard deviation of the transverse deviation angle $\Delta\beta_p^+$ on the transverse incident angle β_p^-.

Sommerfeld and Huber [8] carried out measurements of particle rebound angles $\alpha_{p,xy}^+$ for particle vertical incident angles with $|\alpha_p^-| \in [0°, 50°]$, since the channel was narrow. However, the absolute value of the particle vertical incident angle $|\alpha_p^-|$ is expected to be larger for example in particle-laden flow in a pipe bend. Therefore, Fig. 17 shows mean values and standard deviations of the generated transverse deviation angle in the case of anisotropic surfaces (2D roughness and roughness with high anisotropy), for $|\alpha_p^-| \in [0°,90°]$. The particle transverse incident angle is chosen to be $\beta_p^- = 60°$, so that the particle vertical incident plane is not collinear with either of the two principal directions of roughness. The mean values of the transverse deviation angle for isotropic surfaces are zero and this case is not shown in Fig. 17.

For the rebound of particles from the examined rough walls, the mean value and standard deviation of the particle transverse deviation angle, $E(\beta_p^+ - \beta_p^-)$ and $\Delta\beta_p^+$, respectively, increase with increase in the absolute value of the particle incident angle $|\alpha_p^-|$. This increase is greater for larger particle vertical incident angles α_p^- ($|\alpha_p^-| \gg \Delta\xi$ and $\Delta\zeta$).

For the rebound of particles from a 2D rough wall, the mean value of the transverse deviation angle $E(\beta_p^+ - \beta_p^-)$ is positive for every particle vertical incident angle α_p^-. This mean value is of the order of a few degrees for $|\alpha_p^-| \in [0°,60°]$. On the other hand, for the case of a virtual wall with high roughness anisotropy, the mean value of the transverse deviation angle $E(\beta_p^+ - \beta_p^-)$ is negative for every particle vertical incident angle α_p^-. The mean value of the transverse deviation angle for a wall with high roughness anisotropy is of the order of a few degrees up to the absolute value of the particle vertical incident angle $|\alpha_p^-| = 45°$.

Fig. 17 also shows that for particles bouncing from a wall with high roughness anisotropy there is a more pronounced increase in the mean value and standard deviation of the particle transverse deviation angle, $E(\beta_p^+ - \beta_p^-)$ and $\Delta\beta_p^+$, respectively, for larger particle vertical incident angles α_p^- ($|\alpha_p^-| \gg \Delta\xi$ and $\Delta\zeta$) in comparison with that for particles bouncing from a 2D rough wall, for the same virtual wall normal vector angle standard deviation in the flow direction, $\Delta\xi$, of these two walls and the same particle incident angles.

The agreement between the stochastic and deterministic simulations is very good in all numerical simulations.

5. Conclusion

This paper describes a procedure to generate an anisotropic rough wall, according to Garcia and Stoll [30], and a link of this procedure to virtual rough wall modelling was found. Deterministic simulations of ideally elastic particle rebound from an anisotropic rough wall support statistical modelling of the virtual wall normal vector angles "seen" by particles.

Virtual rough wall normal vector angles are modelled using wall inclination angles, γ and γ^*, defined in the particle incident plane and the orthogonal plane, respectively. It is found that at large particle vertical incident angles α_p^- ($|\alpha_p^-| \gg \Delta\xi$ and $\Delta\zeta$) and any particle transverse angle β_p^-, particles "see" a pair of angles γ and γ^* that obey a Bivariate Normal distribution. At small particle vertical incident angles α_p^- (of the order of $\Delta\xi$ and $\Delta\zeta$) the angle γ is influenced by the shadow effect whereas the angle γ^* is not directly influenced by this effect. The mechanism of multiple particle-wall collisions is accounted for using a direct extension of the modelling approach proposed by Konan et al. [9].

A stochastic model in a Lagrangian frame for the rebound of particles from an anisotropic rough wall is proposed. The proposed model is of general character: it reduces to the 2D model of Konan et al. [9] (if the roughness is 2D) and also to the case of 3D particle rebound from an isotropic wall according to Radenkovic and Simonin [29] (if the roughness is isotropic). The proposed stochastic model for particle rebound from an anisotropic rough wall is compared with deterministic simulations and the experimental results of Sommerfeld and Huber [8].

Deterministic and stochastic simulations show that, when a particle impacts on an anisotropic wall, if the particle vertical incident plane is collinear with either of the two principal directions of an anisotropic rough wall, the mean value of the bouncing particle transverse deviation angle $E(\beta_p^+ - \beta_p^-)$ is zero for any particle incident angle α_p^-. In contrast, if the particle vertical incident plane is not collinear with one of the two principal directions of roughness, then the mean value of the bouncing particle transverse deviation angle is not zero and represents a deflection of the particle path towards the principal direction of low roughness. This effect could be important in pneumatic conveying in narrow channels if the principal direction of wall roughness is not collinear with the mean gas flow direction, considering that the transverse deviation angle occurs for every particle rebound from a wall and may lead to a significant transverse deviation of the particle flow with respect to the mean gas flow direction. To investigate such an effect, a DNS/DPS study of such particle-laden channel flows is suggested, in addition to experimental investigations.

In future work, the joint effect of incident particle rotation and anisotropic roughness on the properties of particle transverse deviation angles should be examined.The link between roughness parameters, particle diameter and standard deviation of virtual wall normal vector angles seen by particles will be investigated. Numerical studies of particle-laden flows in pipes are also suggested to investigate the influence of rough wall anisotropy in such flows.

Credit author statement

Darko Radenkovic: Investigation, Formal analysis, Vizualisation, Writing - Original Draft.

Olivier Simonin: Conceptualization, Methodology, Formal analysis, Writing - Review & Editing.

Declaration of Competing Interest

The authors declare that they have no known competing financial interests or personal relationships that could have appeared to influence the work reported in this paper.

Acknowledgements

The work of the first author was supported by the Ministry of Education, Science and Technological Development of the Republic of Serbia, Project No. TR 35046, and this support is gratefully acknowledged.

References

[1] M. Sommerfeld, Analysis of collision effects for turbulent gas-particle flow in a horizontal channel: part I. particle transport, Int. J. Multiphase Flow 29 (2003) 675–699.
[2] S. Laín, M. Sommerfeld, Euler/Lagrange computations of pneumatic conveying in a horizontal channel with different wall roughness, Powder Tech. 184 (1) (2008) 76–88, https://doi.org/10.1016/j.powtec.2007.08.013.
[3] M. Sommerfeld, J. Kussin, Wall roughness effects on pneumatic conveying of spherical particles in a narrow horizontal channel, Powder Tech. 142 (2004) 180–192, https://doi.org/10.1016/j.powtec.2004.05.002.
[4] M. Benson, T. Tanaka, J. Eaton, Effects of wall roughness on particle velocities in a turbulent channel flow, ASME J. Fluids Eng. 127 (2005) 250–256.

[5] B. Griffiths, Manufacturing Surface Technology: Surface Integrity and Functional Performance, 1st edition Penton Press, London, 2001.
[6] A. Busse, T. Jelly, Influence of surface anisotropy on turbulent flow over irregular roughness, Flow, Turbulence and Combustion, 104, 2020 331–354, https://doi.org/10.1007/s10494-019-00074-4.
[7] Y. Tsuji, T. Oshima, Y. Morikawa, Numerical simulation of pneumatic conveying in a horizontal pipe, KONA 3 (1985) 38–51.
[8] M. Sommerfeld, N. Huber, Experimental analysis and modelling of particle-wall col-lisions, Int. J. Multiphase Flow 25 (1999) 1457–1489.
[9] N.A. Konan, O. Kannengieser, O. Simonin, Stochastic modeling of the multiple re-bound effects for particle-rough wall collisions, Int. J. Multiphase Flow 35 (2009) 933–945.
[10] M. Mando, C. Yin, Euler-Lagrange simulation of gas-solid pipe flow with smooth and rough wall boundary conditions, Powder Tech. 225 (2012) 32–42, https://doi.org/ 10.1016/j.powtec.2012.03.029.
[11] Z. Cheng, M. Zhu, Analyzing the effect of wall roughness on gas-particle flow in con-fined channels based on a virtual-wall-group concept, Int. J. Multiphase Flow 77 (2015) 158–170.
[12] G. Malloupas, B. van Wachem, Large eddy simulation of turbulent particle-laden channel flow, Int. J. Multiphase Flow 54 (2013) 65–75.
[13] K. Squires, O. Simonin, LES-DPS of the effect of wall roughness on dispersed-phase transport in particle-laden turbulent channel flow, Int. J. Heat Fluid Flow 29 (2006) 619–629.
[14] M. Breuer, M. Alletto, F. Langfeldt, Sandgrain roughness model for rough walls within Eulerian-Lagrangian predictions of turbulent flows, Int. J. Multiphase Flow 43 (2012) 157–175.
[15] A. Vreman, Turbulence attenuation in particle-laden flow in smooth and rough channels, J. Fluid Mech. 773 (2015) 103–136.
[16] J.K. Edwards, B.S. McLaury, S.A. Shirazi, Modeling solid particle erosion in elbows and plugged Tees, Journal of Energy Resources Technology 123 (4) (2001) 277–284, https://doi.org/10.1115/1.1413773.
[17] Y. Zhang, E. Reuterfors, B. McLaury, S. Shirazi, E. Rybicki, Comparison of computed and measured particle velocities and erosion in water and air flows, Wear 263 (1) (2007) 330–338, 16th International Conference on Wear of Materials. doi:doi: https://doi.org/10.1016/j.wear.2006.12.048.
[18] D.O. Njobuenwu, M. Fairweather, Modelling of pipe bend erosion by dilute particle suspensions, Computers & Chemical Engineering 42 (2012) 235–247 , European Symposium of Computer Aided Process Engineering - 21 https://doi.org/10.1016/j. compchemeng.2012.02.006.
[19] M. Jafari, Z. Mansoori, M.S. Avval, G. Ahmadi, The effects of wall roughness on erosion rate in gas–solid turbulent annular pipe flow, Powder Technology 271 (2015) 248–254, https://doi.org/10.1016/j.powtec.2014.11.024.
[20] R.E. Vieira, A. Mansouri, B.S. McLaury, S.A. Shirazi, Experimental and computational study of erosion in elbows due to sand particles in air flow, Powder Technology 288 (2016) 339–353, https://doi.org/10.1016/j.powtec.2015.11.028.
[21] Y. Ben-Ami, A. Uzi, A. Levy, Modelling the particles impingement angle to produce maximum erosion, Powder Technology 301 (2016) 1032–1043, https://doi.org/10.1016/j.powtec.2016.07.041.
[22] S. Matsumoto, S. Saito, On the mechanism of suspension of particles in horizontal pneumatic conveying: Monte Carlo simulation based on the irregular bouncing model, Journal of Chemical Engineering of Japan 3 (1) (1970) 83–91.
[23] S. Matsumoto, S. Saito, Monte Carlo simulation of horizontal pneumatic conveying based on the rough wall model, Journal of Chemical Engineering of Japan 3 (2) (1970) 223–230, https://doi.org/10.1252/jcej.3.223.
[24] Y. Tsuji, Y. Morikawa, T. Tanaka, N. Nakatsukasa, M. Nakatani, Numerical simulation of gas-solid two-phase flow in a two-dimensional horizontal channel, Int. J. Multiphase Flow 13 (5) (1987) 671–684.
[25] M. Sommerfeld, G. Zivkovic, Recent advances in the numerical simulation of pneumatic conveying through pipe systems, in: C. Hirsch, J. Periaux, E. Onate (Eds.),Computational Methods in Applied Sciences 1992, pp. 201–212.
[26] A. Konan, S. Badarayani, O. Simonin, K. Squires, LES/DPS of Horizontal Gas-Solid Channel Flow with Particle-Particle Collision and Wall Roughness Effects, in: 6th International Conference on Multiphase Flow, ICMF2007, Germany, Leipzig, 2007 11.
[27] N. Huber, M. Sommerfeld, Modelling and numerical calculation of dilute-phase pneumatic conveying in pipe systems, Powder Tech. 99 (1) (1998) 90–101, https://doi.org/10.1016/S0032-5910(98)00065-5.
[28] N.A. Konan, O. Simonin, K.D. Squires, Detached eddy simulations and particle Lagrangian tracking of horizontal rough wall turbulent channel flow, J. Turbul. 12 (2011) 1–21.
[29] D. Radenkovic, O. Simonin, Stochastic modelling of three-dimensional particle re-bound from isotropic rough wall surface, Int. J. Multiphase Flow 109 (2018) 35–50, https://doi.org/10.1016/j.ijmultiphaseflow.2018.07.013.
[30] N. Garcia, E. Stoll, Monte Carlo calculation for electromagnetic-wave scattering from random rough surfaces, Phys. Rev. Lett. 52 (1984) 1798–1801.
[31] D. Bergström, MySimLabs, http://www.mysimlabs.com 2012 accessed: 11-July-2018.
[32] L. Tsang, J.A. King, K.-H. Ding, Scattering of Electromagnetic Waves: Theories and Applications, John Wiley and Sons, New York, 2000.